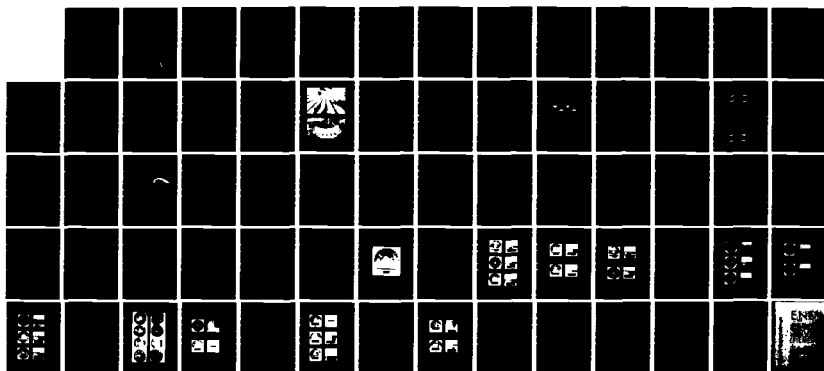AD-A131 581   ASYMMETRIC COLLAPSE OF LOS (LINE-OF-SIGHT) PIPE -- LS-5   1/1
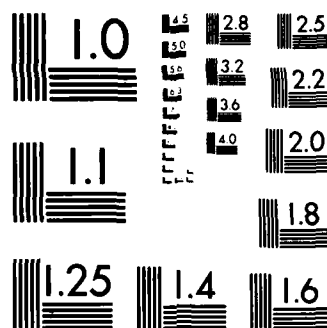   (U) PHYSICS INTERNATIONAL CO SAN LEANDRO CA
               D MUMMA ET AL. 01 MAR 82 PIFR-1517 DNA-6142F
UNCLASSIFIED   DNA001-80-C-0108   F/G 18/3   NL

MICROCOPY RESOLUTION TEST CHART

NATIONAL BUREAU OF STANDARDS-1963 A

AD A131581

ASYMMETRIC COLLAPSE OF LOS PIPE—LS-5

D. Mumma   R. Funston

J. Thomsen   E. T. Moore, Jr.

Physics International Company

2700 Merced Street

San Leandro, California 94577

1 March 1982

Final Report for Period 1 March 1981—1 March 1982

DTIC
ELECTE
AUG 1 9 1983
S
B

Prepared for
   Director
DEFENSE NUCLEAR AGENCY
Washington, DC 20305

DTIC FILE COPY

83 08 18 010

REPORT DOCUMENTATION PAGE	READ INSTRUCTIONS BEFORE COMPLETING FORM	
1. REPORT NUMBER DNA 6142F	2. GOVT ACCESSION NO. AD-A131 581	3. RECIPIENT'S CATALOG NUMBER
4. TITLE (and Subtitle) ASYMMETRIC COLLAPSE OF LOS PIPE — LS-5	5. TYPE OF REPORT & PERIOD COVERED Final Report for Period 1 Mar 81—1 Mar 82	
	6. PERFORMING ORG. REPORT NUMBER PIFR-1517	
7. AUTHOR(s) D. Mumma R. Funston J. Thomsen E. T. Moore, Jr.	8. CONTRACT OR GRANT NUMBER(s) DNA 001-80-C-0108	
9. PERFORMING ORGANIZATION NAME AND ADDRESS Physics International Company 2700 Merced Street San Leandro, California 94577	10. PROGRAM ELEMENT, PROJECT, TASK AREA & WORK UNIT NUMBERS Subtask J24AAXYX983-75	
11. CONTROLLING OFFICE NAME AND ADDRESS Director Defense Nuclear Agency Washington D.C. 20305	12. REPORT DATE 1 March 1982	
	13. NUMBER OF PAGES 66	
14. MONITORING AGENCY NAME & ADDRESS(if different from Controlling Office)	15. SECURITY CLASS. (of this report) UNCLASSIFIED	
	15a. DECLASSIFICATION/DOWNGRADING SCHEDULE N/A since UNCLASSIFIED	
16. DISTRIBUTION STATEMENT (of this Report) Approved for public release; distribution unlimited.		
17. DISTRIBUTION STATEMENT (of the abstract entered in Block 20, if different from Report)		
18. SUPPLEMENTARY NOTES This work was sponsored by the Defense Nuclear Agency under RDT&E RMSS Code B345080462 J24AAXYX98375 H2590D.		
19. KEY WORDS (Continue on reverse side if necessary and identify by block number) LOS Flow Simulation Particulate Jetting		

20. ABSTRACT (Continue on reverse side if necessary and identify by block number)

This report describes the results of a laboratory experiment, designated LS-5, performed to further evaluate the feasibility of using asymmetries to suppress jetting in line-of-sight (LOS) pipes collapsed by the ground shock from an underground nuclear test. Underground conditions were simulated using a sphere of high explosive to collapse small-scale LOS models embedded in saturated sand.

DD FORM 1473 JAN 73   EDITION OF 1 NOV 65 IS OBSOLETE

20. ABSTRACT (cont.)

Three tapered models were evaluated for the first time in this experiment to determine the sensitivity of jet flow to the degree of taper. Several asymmetries were tested, including a model of the LOS pipe planned for HURON LANDING.

In addition to the tapered LOS models, straight LOS pipe models were tested with various internal helix and ring asymmetries to provide further insight into the mechanisms that make these particular designs so effective in attenuating the penetrating jet material.

Aluminum witness plates at the end of the tapered LOS pipe models showed ring-like penetration craters, increasing in diameter with increasing pipe taper. The volume of the target craters was almost constant, even when the taper angle was increased by a factor of four, and this volume was within the spread of volumes measured on witness plates from straight pipe models. The addition of a helix, including that of the HURON LANDING configuration, reduced crater damage; however, the benefit was not as dramatic as that observed for straight pipes, and it decreased as the taper angle increased. Crater damage, ring-like for tapered models without helical asymmetries, was more axial when helices were used.

Experimental results for straight tube LOS models indicated that asymmetries firmly attached to the inside walls of the model were not as effective in attenuating the jet flow as loose asymmetries. Ring asymmetries do not appear to be as effective as helical asymmetries.

The model correlated with the four previous experiments showed an unexpected absence of target penetration, though active instrumentation indicated normal performance. Pretest difficulties suggested that the model may have contained water vapor and possibly some liquid.

Conversion factors for U.S. customary to metric (SI) units of measurement.

To Convert From	To	Multiply By
angstrom	meters (m)	1.000 000 X E -10
atmosphere (normal)	kilo pascal (kPa)	1.013 25 X E +2
bar	kilo pascal (kPa)	1.000 000 X E +2
barn	meter^2 (m^2)	1.000 000 X E -28
British thermal unit (thermochemical)	joule (J)	1.054 350 X E +3
calorie (thermochemical)	joule (J)	4.184 000
cal (thermochemical)/cm^2	mega joule/m^2 (MJ/m^2)	4.184 000 X E -2
curie	*giga becquerel (GBq)	3.700 000 X E +1
degree (angle)	radian (rad)	1.745 329 X E -2
degree Fahrenheit	degree kelvin (K)	$t_K = (t°f + 459.67)/1.8$
electron volt	joule (J)	1.602 19 X E -19
erg	joule (J)	1.000 000 X E -7
erg/second	watt (W)	1.000 000 X E -7
foot	meter (m)	3.048 000 X E -1
foot-pound-force	joule (J)	1.355 818
gallon (U.S. liquid)	meter^3 (m^3)	3.785 412 X E -3
inch	meter (m)	2.540 000 X E -2
jerk	joule (J)	1.000 000 X E +9
joule/kilogram (J/kg) (radiation dose absorbed)	Gray (Gy)	1.000 000
kilotons	terajoules	4.183
kip (1000 lbf)	newton (N)	4.448 222 X E +3
kip/inch^2 (ksi)	kilo pascal (kPa)	6.894 757 X E +3
ktap	newton-second/m^2 (N-s/m^2)	1.000 000 X E +2
micron	meter (m)	1 000 000 X E -6
mil	meter (m)	2.540 000 X E -5
mile (international)	meter (m)	1.609 344 X E +3
ounce	kilogram (kg)	2.834 952 X E -2
pound-force (lbs avoirdupois)	newton (N)	4.448 222
pound-force inch	newton-meter (N·m)	1.129 848 X E -1
pound-force/inch	newton/meter (N/m)	1.751 268 X E +2
pound-force/foot^2	kilo pascal (kPa)	4.788 026 X E -2
pound-force/inch^2 (psi)	kilo pascal (kPa)	6.894 757
pound-mass (lbm avoirdupois)	kilogram (kg)	4.535 924 X E -1
pound-mass-foot^2 (moment of inertia)	kilogram-meter^2 (kg·m^2)	4.214 011 X E -2
pound-mass/foot^3	kilogram/meter^3 (kg/m^3)	1.601 846 X E +1
rad (radiation dose absorbed)	**Gray (Gy)	1.000 000 X E -2
roentgen	coulomb/kilogram (C/kg)	2.579 760 X E -4
shake	second (s)	1.000 000 X E -8
slug	kilogram (kg)	1.459 390 X E +1
torr (mm Hg, 0° C)	kilo pascal (kPa)	1.333 22 X E -1

*The becquerel (Bq) is the SI unit of radioactivity; 1 Bq = 1 event/s.
**The Gray (Gy) is the SI unit of absorbed radiation.

A more complete listing of conversions may be found in "Metric Practice Guide E 380-74," American Society for Testing and Materials.

CONTENTS

ILLUSTRATIONS

ILLUSTRATIONS (cont.)

SECTION 1

INTRODUCTION

1.1 BACKGROUND

The line-of-sight (LOS) pipe flow observed on underground
nuclear test (UGT) experiments fielded by the Defense Nuclear
Agency (DNA) consists of at least three parts: (1) a plasma
pulse recorded very close to zero time, (2) a later time plasma
jet, and (3) a jet of particulate or mixed phase material. The
latter two parts are caused by the ground-shock-induced collapse
of the LOS pipe. These jets are of concern in the DNA UGT
containment program because they can severely damage LOS pipe
closure mechanisms. Elimination or substantial suppression of
the jets would protect close-in experiment stations from blast
and high velocity debris, and would generally further enhance the
containment prospects for LOS events.

Physics International Company is conducting an effort to
test LOS pipe designs in laboratory experiments. The objectives
of these experiments are to: (1) examine formation of the LOS
pipe ground-shock-induced collapse jet, (2) determine ways of
minimizing or inhibiting jet formation, and (3) test the effec-
tiveness of various LOS pipe designs in attenuating jetted
flow. Work to date has used only thin, stainless steel, straight
tubes to represent LOS pipes to minimize geometry variables and
reduce fabrication complexities. Up to 26 pipe models have been

embedded in saturated sand around a sphere containing high explosive in each experiment. Detonation of this explosive causes the pipes to collapse and to form jets.

Significant results from previous experiments (References 1 through 3) have shown that straight LOS pipe models always form jets when collapsed by the shockwave in the surrounding sand. The collapse process appears to stop producing penetrating[*] jets when 60 cm or more of the LOS model are plugged. The first 60 cm of LOS pipe length is referred to as the "source," or jet-generating region of the model. Although most models are evac-uated to a vacuum of a few microns, models at atmospheric pres-sure produce similar results. These models are referred to as "standard" models without asymmetries. If the LOS model wall thickness is increased, more energetic jets are produced.

To date we have been unsuccessful in determining practical techniques to inhibit formation of these jets by asymmetrical design. Materials of different densities were added to the out-side of the pipe in many different configurations to alter the direction of wall collapse or to redirect the resulting jet into the pipe wall, but without promising results.

The addition of spiral ribbons (helices) to the inside sur-face of the tube proved effective in attenuating the penetrating

---

[*] The primary method for determining the strength of the penetrating jet has been to measure the depths and volumes of penetration craters formed in thick aluminum targets placed at the end of each LOS pipe model.

jet. The attenuation mechanism appears to be independent of the material (steel, lead, or plastic) used for the helix and is still effective when the helix thickness is reduced to that of the tube wall thickness. The helix is still effective when a short helix is located in the tube well beyond the collapse region where penetrating jets are formed--the "flow" region of the pipe.

1.2 EXPERIMENT OBJECTIVES

The principal objectives of this effort were to: (1) evaluate the jet energy produced by tapered LOS pipe models, more closely simulating LOS pipes fielded on UGT experiments, (2) determine whether the use of helical asymmetries placed on the inside surface of these tapered pipes is as effective as was observed for straight pipes, including a helical asymmetry design installed in HURON LANDING LOS pipe, and (3) continue to increase the database on helical asymmetries in straight pipes to help resolve the phenomenology of jet generation and attenuation.
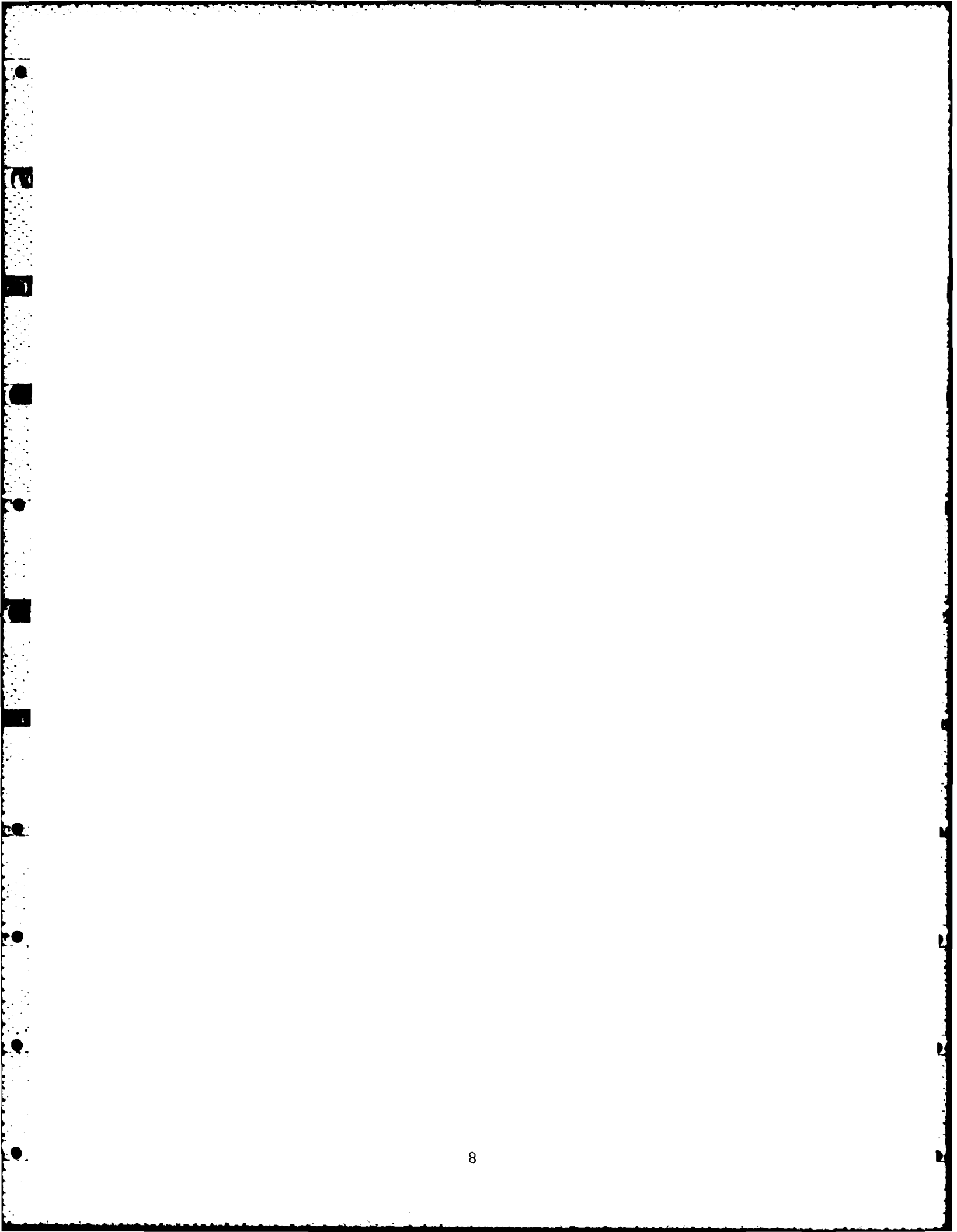
SECTION 2

DESCRIPTION OF EXPERIMENT (LS-5)

2.1 CONCEPT

The LS-5 experiment was devised to simulate conditions that
exist during the collapse of a line-of-sight (LOS) pipe in an
underground nuclear test (UGT). This experiment consisted of 20
small steel tubes positioned radially around a sphere containing
liquid high explosive and embedded in saturated sand. The tubes,
explosive, and sand represented, respectively, the LOS pipes, the
nuclear device, and the geological medium in a UGT. Configura-
tion of this experiment is shown schematically in Figure 1.
Individual components of the experiment are described below.

2.2 EXPERIMENTAL APPARATUS

2.2.1 Explosive Source. The explosive source is shown in
Figure 2. Approximately 136 kg of liquid nitromethane was con-
tained in a 61.0-cm-diameter fiberglass sphere. This explosive
has a detonation pressure of 14 GPa (140 kbar), comparable to the
calculated peak free-field radial stress at a range of interest
for a nuclear event such as MIGHTY EPIC.

A booster assembly initiated detonation in the nitromethane
at the center of the sphere. It was placed into position through
a vertical fill tube at the top of the sphere. The booster

(a)

(b)

Figure 1. Spherical high explosive experiment for investigating the effects of asymmetries in the LS-5 experiment : (a) plan view, and (b) cross section.
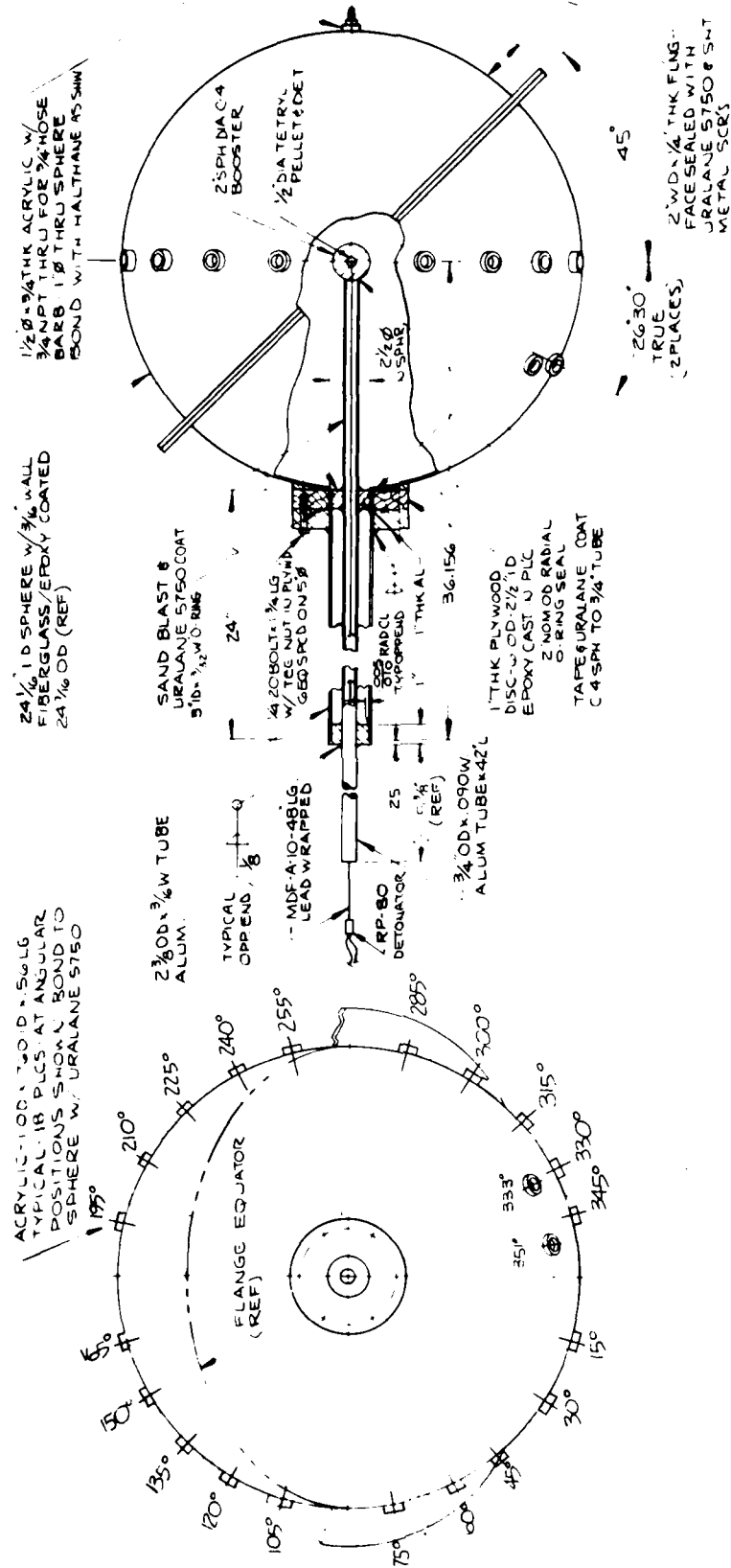
10

Figure 2. Explosive source used in LS-5.

assembly was an explosive train consisting of a composition C-4 explosive molded into a small sphere, a 1.25-cm-diameter tetryl pellet located at the center of the sphere, and a length of mild detonating fuse (MDF) that extended beyond the top of the fill tube. The detonation sequence in the explosive train was initiated by an RP-80 exploding bridgewire detonator located at the end of the fuse.

When the test was first conducted, the detonator fired and ignited the MDF, but the MDF failed to ignite the booster assembly. The nitromethane was drained from the sphere, the booster assembly was rebuilt with the detonator placed directly in the center of the booster, and the length of MDF was eliminated. This alternate configuration successfully detonated the nitromethane.

2.2.2 LOS Models. The standard straight models were fabricated from 19-mm-diameter, 0.305-mm-thick welded and drawn AISI 321 stainless steel tubes (Military Specification T-8808). The tapered tubes were fabricated by forming flat sheets of 0.305-mm-thick sheets of 321 stainless steel into cones of the desired angle, and electron-beam welding the seam. After the tubes were cut to the desired length a steel plug was bonded onto the end of the tube facing the explosive sphere. An aluminum flange bonded onto the opposite end of each tube supported a thin Mylar diaphragm and vacuum port. Aluminum targets were placed against the flange of each model.

As shown in Figure 1, the models were designated either by title or by a model number, which was also the position around

the explosive sphere. Twenty LOS models, located in the horizontal midplane of the sphere, were inserted into precisely located Lucite positioning rings on the surface of the explosive sphere and carefully aligned perpendicular to this surface.

2.2.3 <u>Test Bed</u>. The saturated sand test bed was contained in a cylindrical steel tank. The tank was formed by rolling and welding a 6.4-mm-thick steel plate into a 2.44-meter-diameter steel cylinder and reinforcing the top and bottom of the tank with U-channel. The tank then was placed on a concrete pad. The LOS models and instrumentation lines were positioned radially from the explosive sphere, located at the center of the tank (see Figure 3a).

The test bed was prepared by carefully pouring sacks of Monterey sand into water controlled by a water distribution system around the perimeter of the tank bottom. The water distribution system consisted of perforated plastic tubing in a bed of pea-sized gravel. Care was taken to maintain a thin slurry of sand and water in the tank at all times. The slurry was hand-mixed to assure thorough wetting of the sand grains and to avoid trapping of air bubbles. Figure 3b shows the experimental setup after the tank has been filled with sand.

The instrumentation for determining the time-of-arrival (TOA) of the shock wave in the saturated sand was located at positions 0 and 180 deg (Figure 2). Similarly, the horizontal plane of positions 90 and 270 degrees contained the flange joint

(a) Nitromethane sphere and LOS pipe models
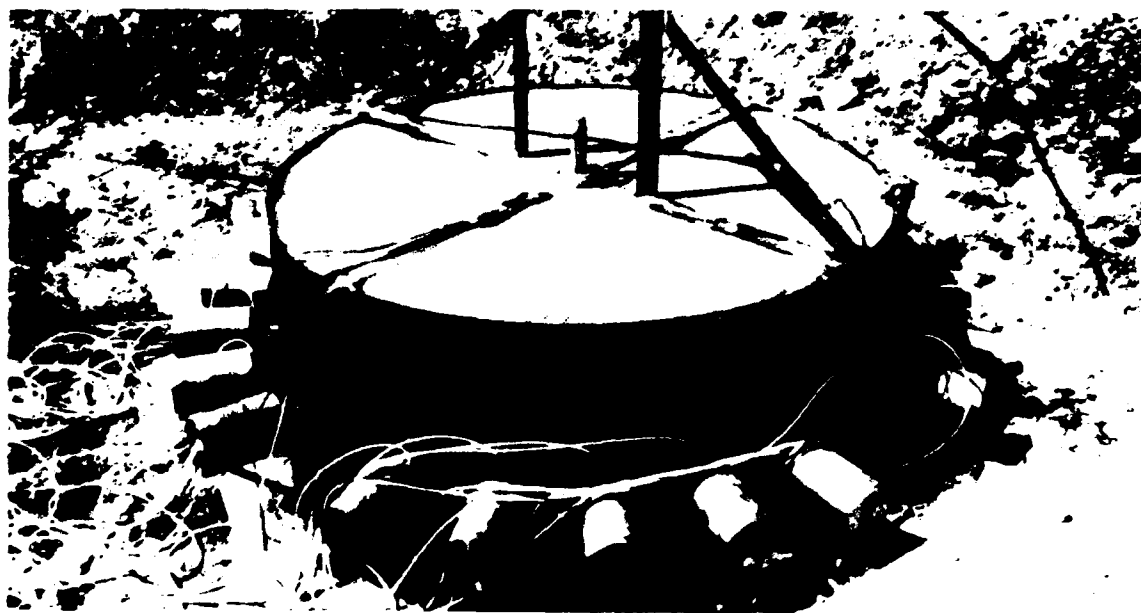
(b) Test bed filled with saturated sand

Figure 3. The LS - 5 test geometry (20 LOS pipe models).

for the two fiberglass hemispheres that formed the explosive sphere. The flange was oriented at a 45 degree angle with respect to the horizontal plane.

2.3 LOS MODEL DESCRIPTION

The LOS pipe models used in this experiment are listed in Table 1 and pictured in Figure 4. Two similar models were tested when penetrating jets were expected because of the large scatter in penetration data obtained in previous experiments. The table provides a brief description of each model, its position in the test bed, the relevant dimensions of the models, and the salient dimensions of any asymmetries included in the model. The configuration and nomenclature for the helical and ring asymmetries used in this experiment are shown in Figure 5. Three taper half-angles were used. The baseline half-angle (standard taper) was 0.375 degrees. The other two angles were 2 times and 4 times this angle, or 0.75 degrees and 1.5 degrees, respectively. The 20 models can be categorized by technical objective as described in the following subsections.

2.3.1 <u>Reproducibility of a Standard Model (Model 1)</u>. One standard model with a straight tube and no asymmetry was used as a baseline to compare its results with eight similar models used in four previous experiments (LS-1 through -4).

2.3.2 <u>Tapered Pipes Without Asymmetries (Models 2, 3, 5, 6, 8, and 9)</u>. Three pipe tapers were selected to test whether these pipes would produce jets and craters similar to those observed in previous experiments with straight tubes. A tube half-angle of

Table 1 Description of LOS pipe models tested in the LS-5 experiment.

LOS Model	Model Number and Position	Characteristics of Asymmetry or Other Jet Attenuation Mechanism					Notes
		Material	Width (mm)	Thickness (mm)	Length (mm)	Pitch (mm)	
Standard Tube	1	--	--	--	--	--	19 mm OD, 0.3 mm wall thickness
2/1X Standard Tube	17 & 18	--	--	--	--	--	13 mm OD, 0.25 mm wall thickness
Standard Tube/Asymmetry							
Solid Rings	12	Steel	15.9	0.40	384	51	
Soldered Wire Helix	13	Steel	0.4	0.40	384	51	
Soldered Helix	14	Steel	15.9	0.40	384	51	
Loose Rings	15	Steel	15.9	0.40	384	51	
Expansion Chamber/Rings	16	Steel	15.9	0.40	384	51	
0.375° Half-Angle Taper Tube							
Std. Taper	2 & 3	--	--	--	--	--	
Std. Taper/Helix	4	Stainless Steel	15.9	0.30	994	51	
Std. Taper/HURON LANDING Helix	19	Stainless Steel	15.9-26.5	0.30	994	51-86	Variable pitch and width
Std. Taper/Ext Lead-Foam Helix	20	Stainless Steel	6.35	6.35	994	12.7	Alternating lead and foam spirals
0.75° Half Angle Taper Tube							
5X Taper	5 & 6	--	--	--	--	--	
2X Taper/Helix	7	Stainless Steel	15.9	0.30	994	51	
2X Taper/Rings	11	Stainless Steel	15.9	0.30	994	51	
1.5° Half-Angle Taper Tube							
4X Taper	8 & 9	--	--	--	--	--	
4X Taper/Helix	10	Stainless Steel	15.9	0.30	994	51	

16
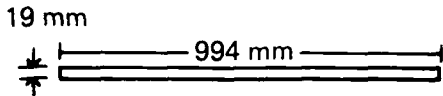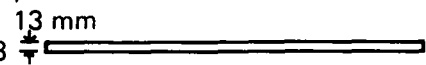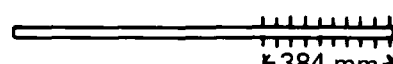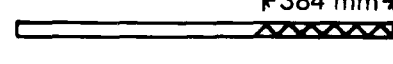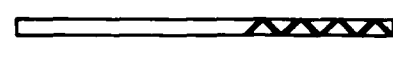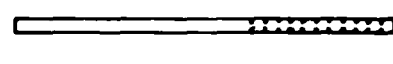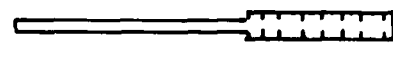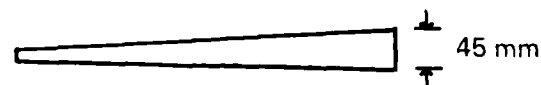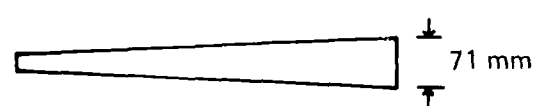
MODEL No.	MODEL CONFIGURATION	MODEL DESCRIPTION

Figure 4. Pictorial configuration of models used in the LS-5 experiment.

THICKNESS
(0.4 mm)

PITCH DISTANCE

(50.8 mm)

WIDTH
(15.9 mm)
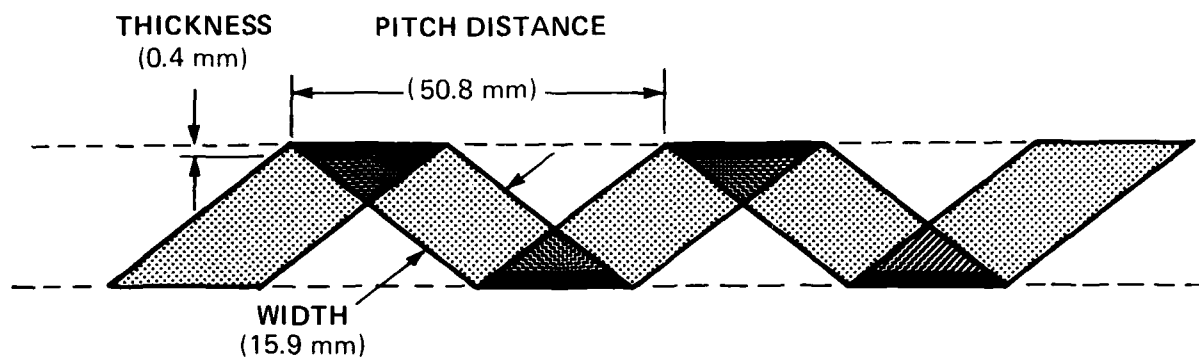
(a)   Configuration of the standard helix asymmetry

THICKNESS
(0.4 mm)

PiTCH DISTANCE

(50.8 mm)

WIDTH
(15.9 mm)
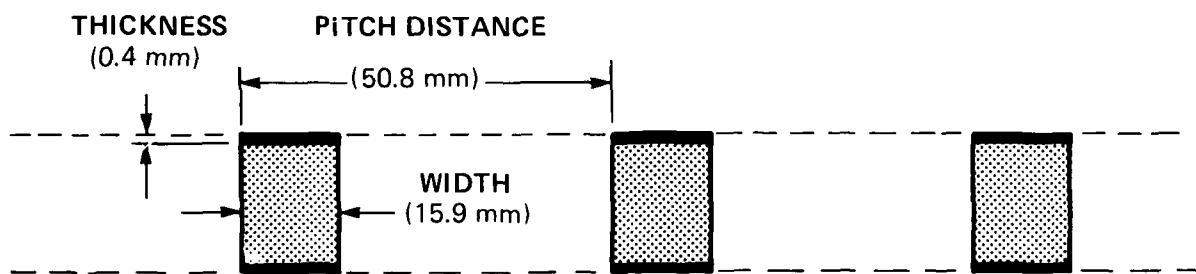
(b) Configuration of the standard ring asymmetry

Figure 5.   Configuration and nomenclature of helical and ring asymmetries.

0.375 degrees was selected as the "standard" taper, closely representing the angle typically used for LOS pipes in UGTs (Models 2 and 3). To evaluate the sensitivity of jet formation to the pipe taper angle, two larger half-angles of 0.75 (2X) and 1.5 (4X) degrees were used for Models 5 and 6, and 8 and 9, respectively.

2.3.3 <u>Tapered Pipes with Internal Asymmetries (Models 4, 7, 10, 11, and 19)</u>. Helices were used in models with the three different tapers (standard taper, 2X standard taper, and 4X standard taper) to determine if helices were as effective in jet attenuation as they were in straight pipes. The helices were used for the full length of the models.

Model 11 incorporated a full-length ring asymmetry in a 2X tapered tube to determine whether rings would be as effective as the helical configuration. Model 11 would be compared to Model 7. Simpler fabrication techniques possibly would favor ring configurations if they are as effective as helices.

A helix is installed in the LOS pipe for HURON LANDING. Model 19 was a close representation of that helical design; results of this test showed that this helix design was as effective as the standard helix in a tapered pipe in attenuating the penetrating jet.

2.3.4 <u>External Helical Asymmetry (Model 20)</u>. One model, Model 20, incorporated an external helical asymmetry to further evaluate whether jet formation could be sufficiently altered or disrupted that the high energy jet flow would be reduced. On the

outside of a 2X tapered pipe, a 6.35-mm square lead bar was spirally wrapped with a 6.35-mm spacing between wraps (12.7-mm pitch). The void spacing was filled with low density foam. This configuration was designed to determine if large areal density variations in the wall thickness might totally prevent jet formation or at least direct the jet into the pipe wall.

2.3.5 <u>Asymmetry Sensitivity to Method of Attachment (Models 12, 13,14, 15, and 16)</u>. From work performed to date, a thin helical or ring asymmetry of a specific design loosely placed in the flow region (near the target) of a straight pipe is shown to be very effective in almost totally eliminating the high-energy jet. There was little knowledge about whether asymmetry width or attachment method would alter performance. The remaining models in this experiment were designed to answer some of these questions and provide a better understanding of the attenuation mechanism. Figure 6 details each model's particular asymmetries. Model 14 incorporated the previously successful standard stainless steel helix design except that the helix was soldered to the wall of the pipe. This model would test whether the nondamaging gas flow ahead of the high energy jet caused the helix to tip towards the axis, more effectively intercepting the jet.

Model 13 used a wire wound into a helix to determine whether the width of the helix is important. The wire diameter was the same thickness as the standard helix (0.4 mm) wound with the standard pitch (50.8 mm) and was soldered to the inside surface of the tube.
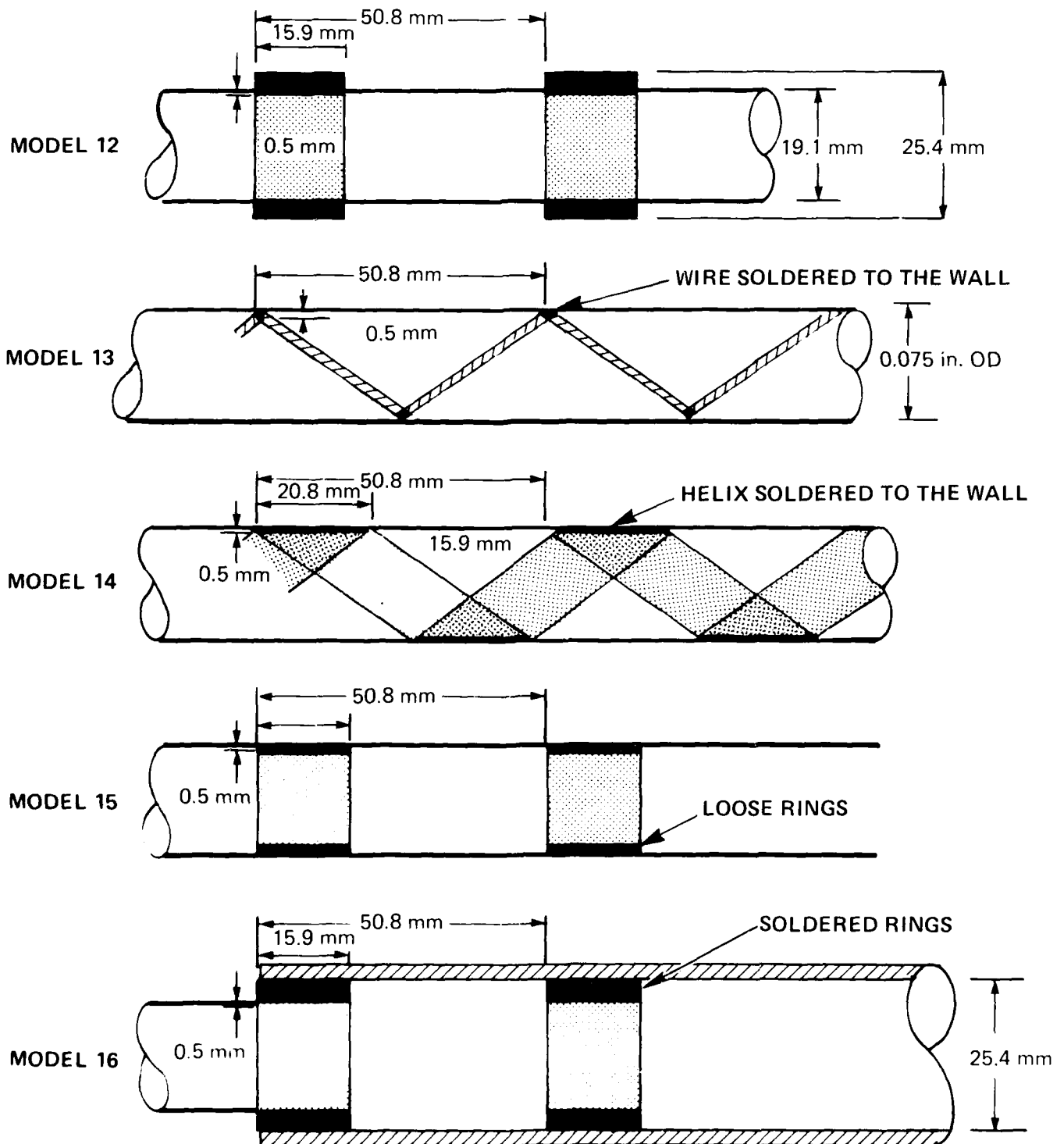
Figure 6. Detail of straight tube asymmetries used on LS-5.

Models 15 and 12 used both loose rings and firmly attached rings to further evaluate the question of attachment method and also provide additional data regarding the effectiveness of rings compared to helices.

The final model, Model 16, was used to provide some understanding of why a ring asymmetry placed in a flow region expansion chamber of the LS-4 experiment was not effective in attenuating the jet. A possible explanation was that the inside diameter of the ring was the same diameter as the pipe; therefore, the jet was not intercepted by the rings if it continued in a straight line through the chamber. For this test the ring diameter was decreased so that it protruded into the cross section of the tube the same amount as standard loose asymmetries inserted into the pipe.

2.3.6 Two-Thirds Diameter Models (Models 17 and 18). To evaluate whether the target damage would scale, two models (17 and 18) were tested with tubes two-thirds the diameter of the standard 1.9-cm diameter tubes. The wall thickness was reduced from the standard of 0.31 mm to 0.25 mm, not quite two-thirds but as close as could be obtained with commercial tubing. The standard 1-meter tube length was maintained.

2.4 MEASUREMENTS

The active instrumentation used in this experiment was directed at determining the time at which the detonation reaches the inside surface of the fiberglass sphere, the trajectory of

the spherically divergent shock wave in the saturated sand, pressure generated inside the models, the velocity of the jets generated in the LOS models, and the rate at which the jet penetrates the aluminum target of several models.

Aluminum targets were placed at the ends of all models to provide passive, terminal evidence of the energy and momentum contained in the jet.

2.4.1 Detonation Wave. Four ionization pins were located on opposite sides of the inside surface of the explosive sphere to measure the time at which the detonation wave reaches this interface. The purpose of this measurement was to assure that the detonation was spherically symmetrical about the point of initiation prior to the detonation entering the saturated sand surrounding the models.

2.4.2 Shock Wave in Test Bed. The trajectory of the spherically divergent shock wave in the saturated sand test bed was determined from TOA measurements. These measurements were obtained from the response of two radial lines of seven piezoelectric pins placed in the saturated sand on opposite sides of the explosive sphere. The pins were located in the horizontal midplane of the sphere and extended from 32.5 to 107.5 cm from the center of the sphere. The first pin of each radial line was located 1.5 cm from the inside surface of the explosive sphere. The intervals between the first and second pins and between the second and third pins were 5 and 10 cm, respectively. Thereafter the interval between pins was 15 cm.

2.4.3 <u>Jet Velocity</u>. Instrumentation for determining jet velocity was included on three models--the standard (Model 1), the 2X taper model (No. 6), and the 2X taper model with helix (No. 7). The instrumentation consisted of five ionization pins placed through the walls of the models at 5-cm intervals and extending from 65 to 85 cm from the steel plug on the end of the model nearest the explosive sphere. The geometry for the ionization pin instrumentation is shown in Figure 7 along with a photograph of a tube with the pins attached.

Impact switches attached to the front of 13 targets measured TOA of the ionized gas flow and the subsequent flow that produced target damage. These switches consisted of a sandwich of two aluminum foils separated by thin Mylar sheets. A 6-mm-diameter hole was cut in the first Mylar sheet, exposing it to the LOS pipe interior so that any ionizing flow would short out the charged foil to the pipe wall, producing a signal. The second foil does not produce a signal until the 0.076-mm-thick Mylar is penetrated. The configuration of these impact switches is shown in Figure 8.

2.4.4 <u>Jet Pressure</u>. To measure the magnitude of the pressure generated by the flow within the pipe, pressure gages were placed in the target mounting flanges (see Figure 9) of three targets. Redundant gages helped confirm that the pressure gages were recording reproducible data. A 5-cm column of oil separated the gage from the inner pipe wall for ease of mounting and to provide temperature and shock isolation. The 13-mm gage port distance from the target face allows observation of the pressure wave before and after reflection from the target face. The gage
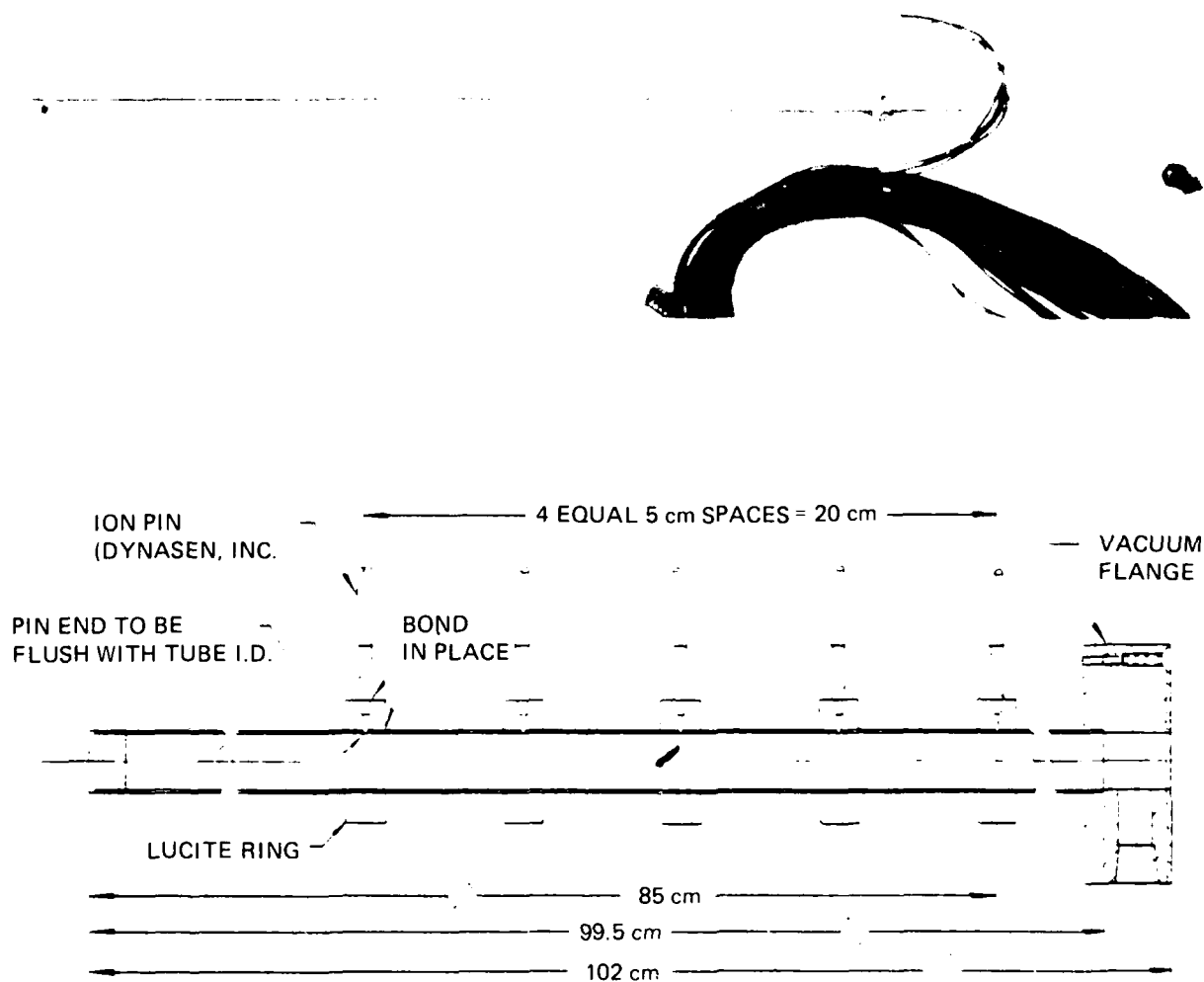
24

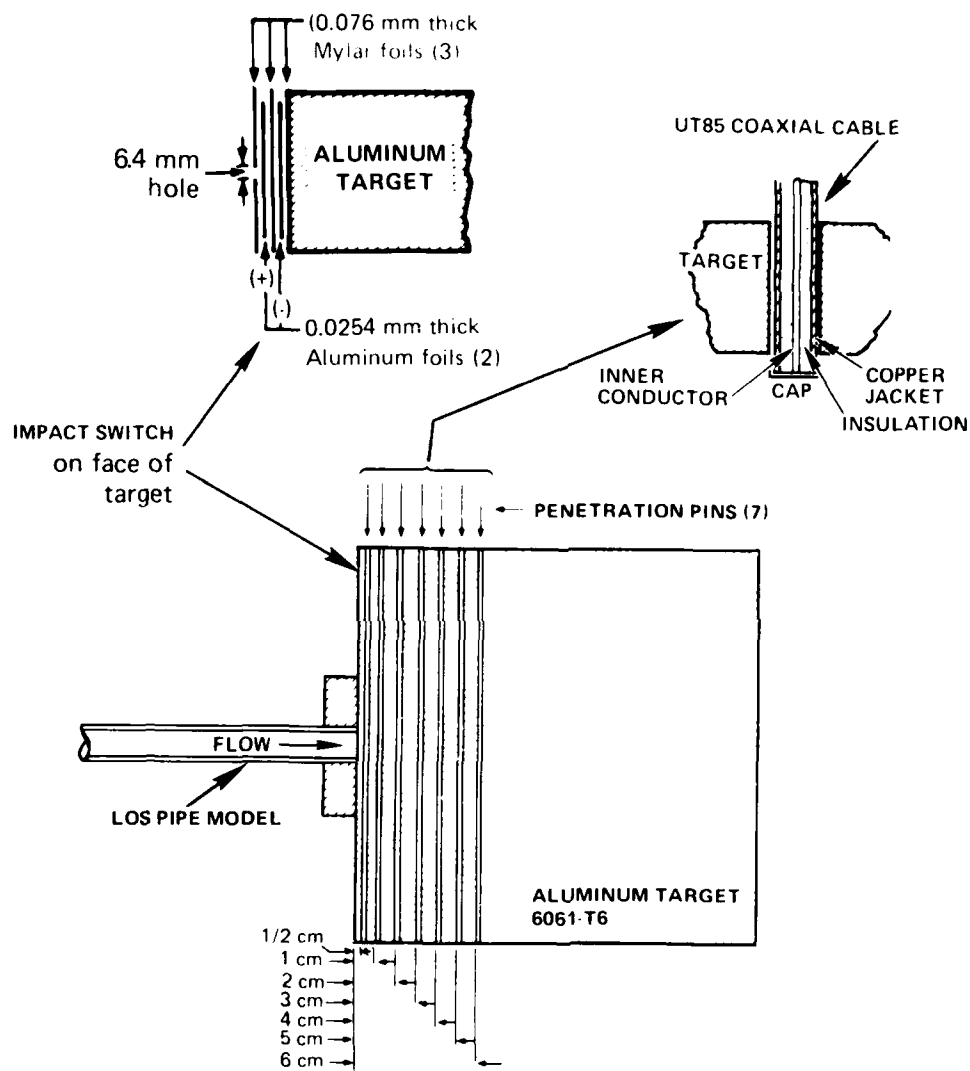Figure 7. Configuration of ionization pins used for jet velocity inside the LOS tubes.

Figure 8. Instrumentation used for measuring the jet TOA at the target face and jet penetration and stress within the target.
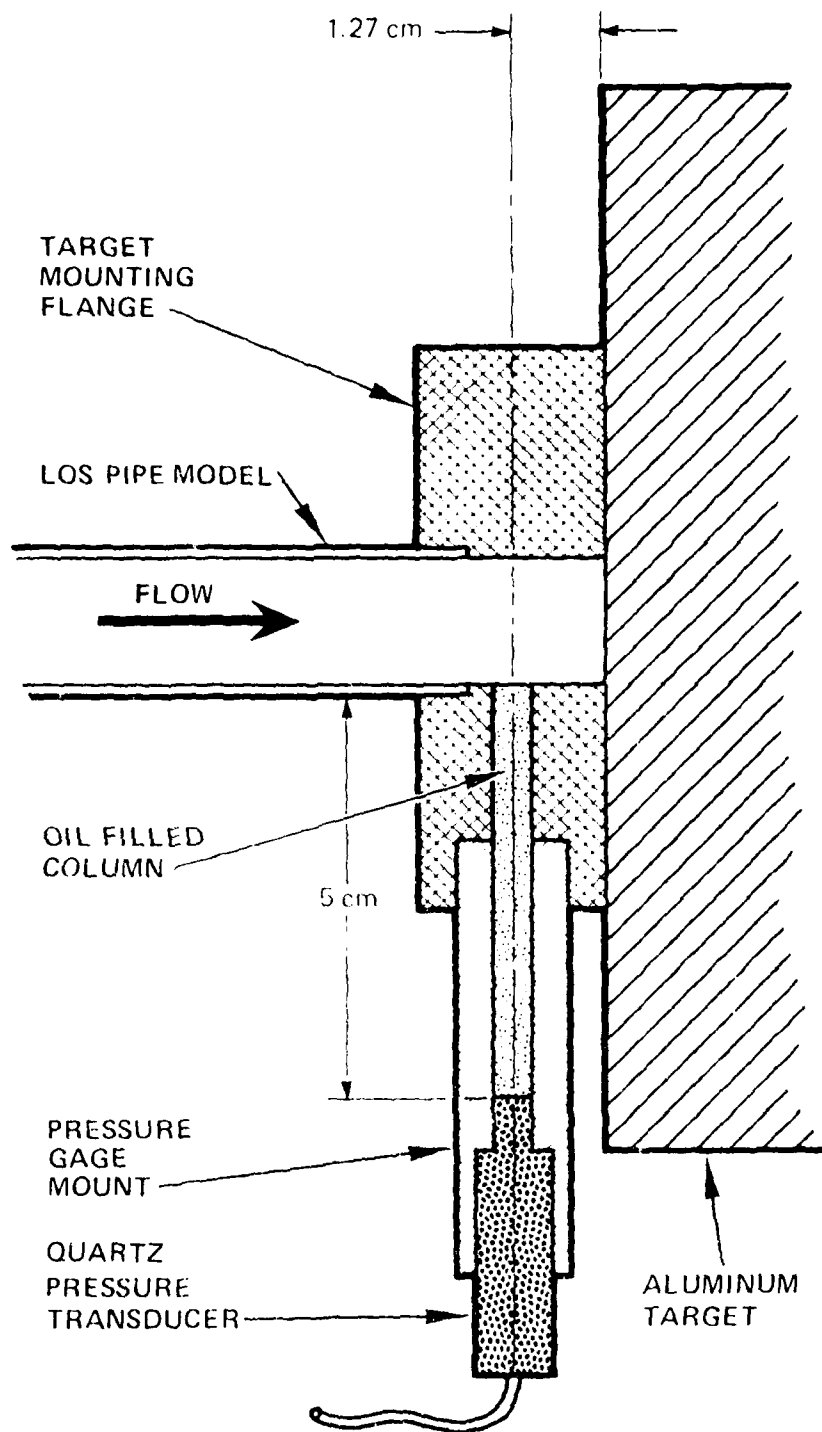
Figure 9 Configuration of typical pressure gage mount

used for these measurements was a PCB Model 109A piezoelectric pressure gage* (PZ gage) with a dynamic range of 0 to 550 MPa (0 to 5.5 kbars).

2.4.5 Rate of Target Penetration. Using the configuration shown in Figure 8, the aluminum targets of three LOS models contained TOA instrumentation to investigate the rate of jet penetration. Six UT 85 coaxial cables were placed in small, tight-fitting holes drilled through the centerline of the target. Successive coaxial cables short out as the jet penetrates the target.

2.4.7 Target Damage. Measurement of the depth and diameter of the craters produced in aluminum targets provided passive evidence of the energy and momentum in the jets. The targets were 20-cm-diameter 6061-T6 aluminum cylinders with a length of 30 cm. They were supported on brackets welded to the outside of the steel test bed tank and positioned against the vacuum flange that enclosed the exit end of each LOS pipe model.

*Manufactured by PCB Piezotronics, Buffalo, NY

SECTION 3

EXPERIMENTAL RESULTS

When this experiment was initially fired, the mild detonating fuse (MDF) firing train failed to detonate the main booster charge of composition C-4 and nitromethane. Inspection of the experimental setup revealed that some targets that were not firmly attached to the line-of-sight (LOS) models were displaced a few centimeters. The sphere containing the nitromethane showed a small leak near the top where the booster assembly was attached. Our initial assessment was that the damage was minimal and the test could be reconducted with a revised booster assembly, which eliminated the use of MDF. The explosive sphere was repaired and test preparations restarted. Just prior to refiring the test, the vacuum of two models (Model 1 and 20) was found to be very poor because of water intrusion. As many of the targets as practical were removed and the internal LOS pipe conditions noted. The data relating to the performance of tapered pipes were needed in timely manner and, since the vacuum of these models was satisfactory, the test was continued without further model repair and was successfully fired.

3.1 DETONATION WAVE

The two ionization pins on the inside surface of the fiberglass sphere showed a 0.2-μs difference in the times at which the detonation wave arrived at four sides of the sphere. Assuming

the detonation velocity in the nitromethane was 0.6 cm/µs, a 0.2-µs difference in arrival times would imply that the detonation wave on one side of the sphere was leading the opposite side by 0.12 cm. This timing difference is probably due to the inability to maintain the shape of the thin-walled fiberglass sphere when it is filled with 136 kg of a liquid and covered with saturated sand. Therefore, for all practical purposes, the detonation was quite symmetrical.

3.2 SHOCK WAVE IN TEST BED

The TOA data for the spherically divergent shock wave along the two PZ pin diagnostic lines are shown in Figure 10. The data for the two lines are almost identical, providing good confidence in the reliability of values obtained. The data also suggest that the test bed was fully saturated, and were similar to the LS-2, LS-3, and LS-4 experiment test bed data shown in Figure 11.

3.3 JET VELOCITY

The TOA data obtained from the ionization pins located in the sidewalls of the three models with this instrumentation were quite good. The trajectories of the best estimated data for the three models with jet velocity pins are shown in Figures 12 through 14. The target foil switch data and penetration data also are shown in these plots.

The first TOA signal from the target switch appears to fit quite consistently with the jet velocity data. There was very
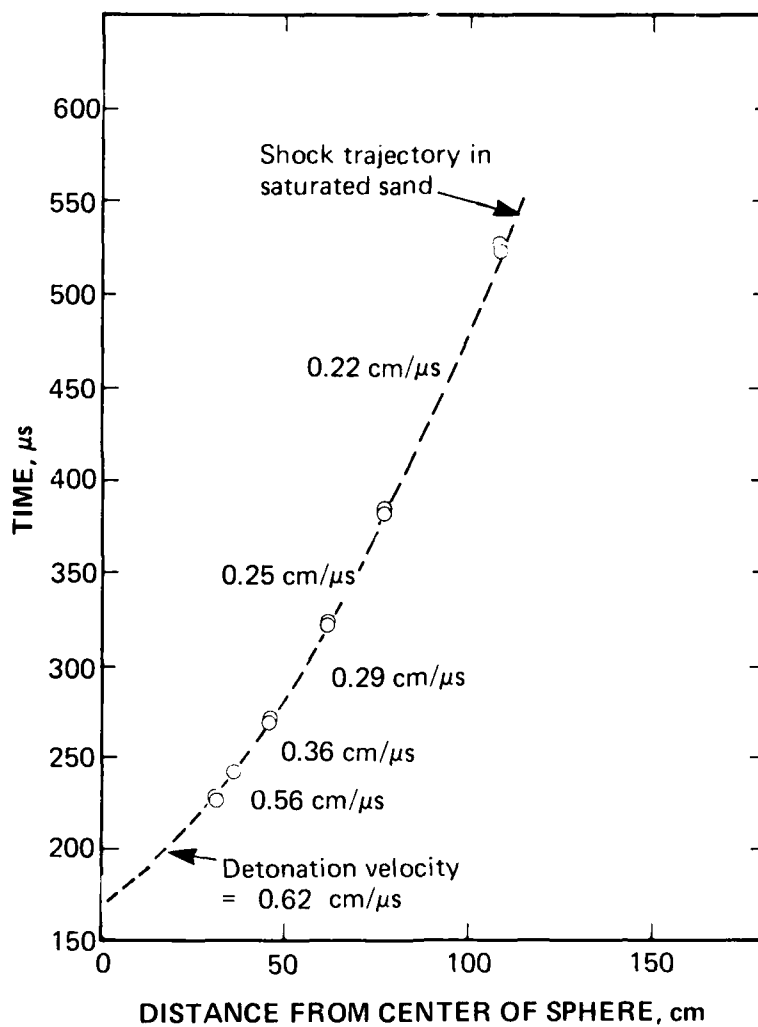
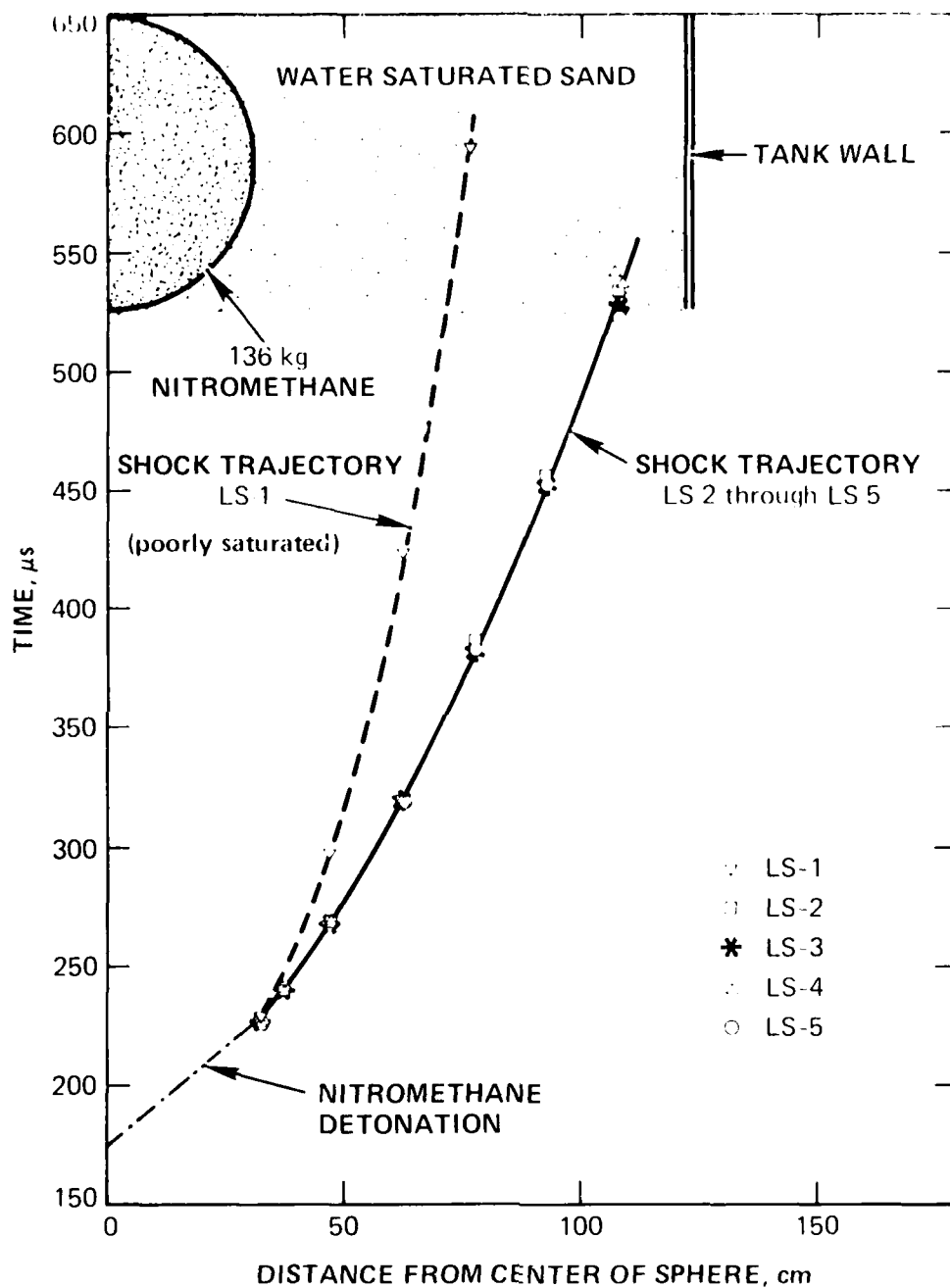Figure 10. Test bed shock wave trajectories in the saturated sand for LS-5.

31

Figure 11 Summary of free field shock trajectories in the LS experiment series.
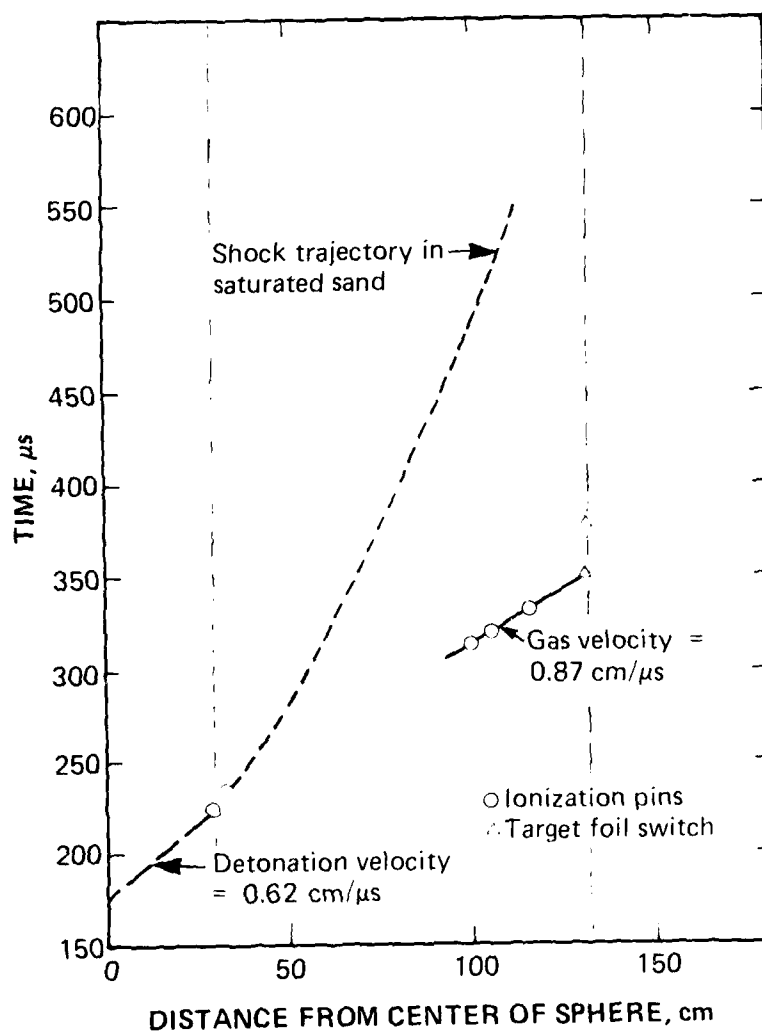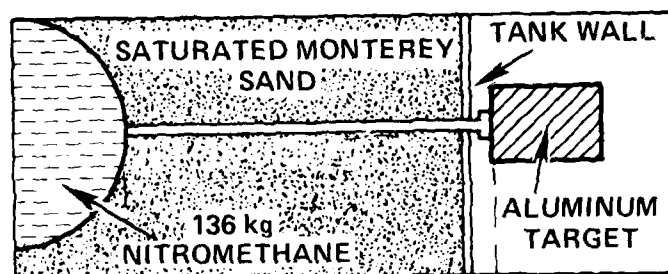
Figure 12. Detonation, shock, and jet trajectories for Model 1 (LS-5).
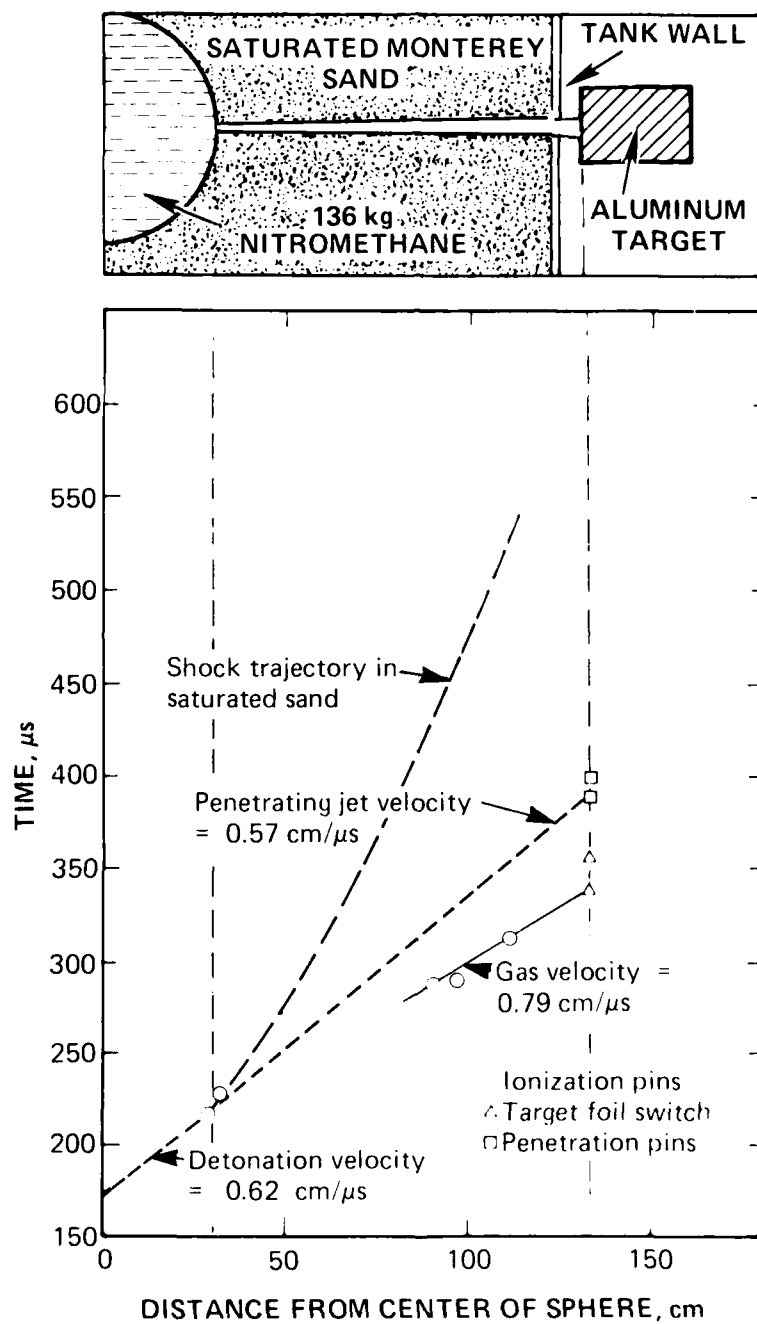
33

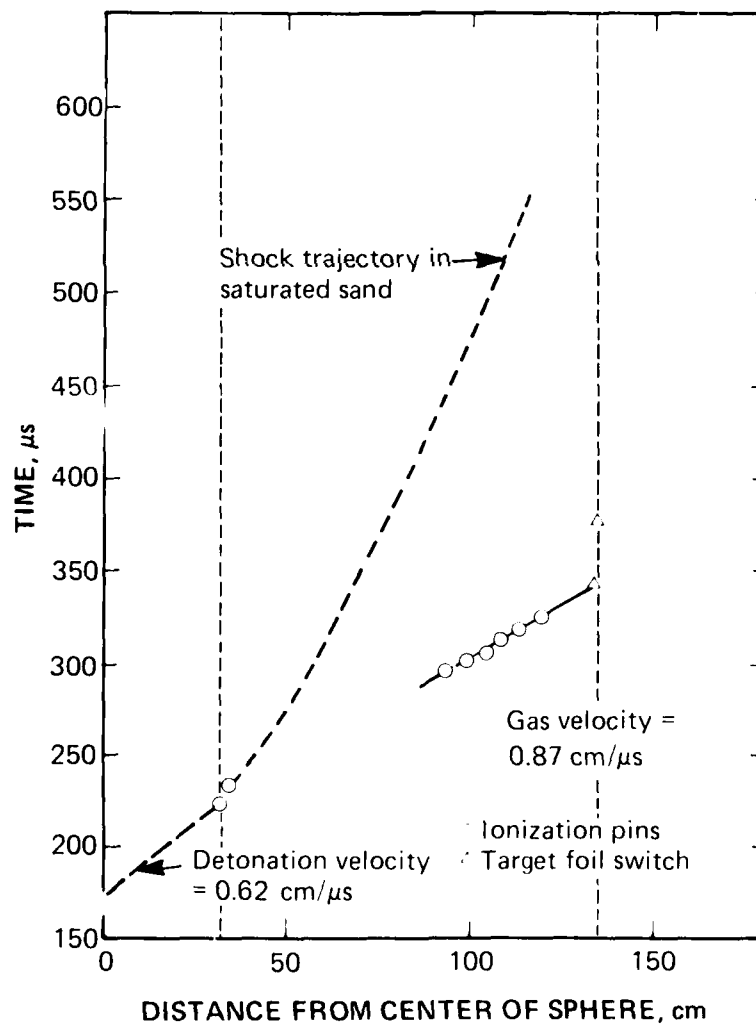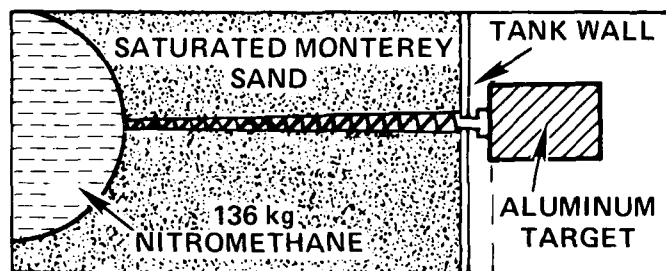Figure 13. Detonation, shock, and jet trajectories for Model 6 (LS-5).

Figure 14. Detonation, shock, and jet trajectories for Model 7 (LS-5).

little correlation between these types of data for Model 1 in the LS-4 experiment. The high jet velocity of 1.2 cm/µs reported for the standard model in that experiment may be suspect.

The second set of TOA pin data for Model 6 does not appear to correlate with the time of target penetration, as was also observed in the LS-4 experiment. As can be seen in Figure 13, the second foil switch reports much earlier than the first penetration pin would suggest it should have. The Mylar thickness should probably be increased slightly in this instrumentation to provide a valid TOA of the penetrating jet.

The target foil TOA data are given in Table 2. The data do not show a consistent trend that could be used to evaluate model performance or the effectiveness of asymmetries, particularly when the time differences between the first and second signals are compared, again confirming that the second TOA of the switch does not produce meaningful data.

3.4 JET PRESSURE

Two quartz pressure gages were located in the LOS model target mounting flanges of three targets to record jet pressure. Unfortunately the data from the LS-4 experiment had not been reduced when this experiment was conducted. From the LS-4 data we concluded that these pressure data are difficult to interpret and may be of somewhat limited value due to pipe expansion, pressure loss at the point where the flange mounts to the target, and the use of the 5-cm-long oil-filled column.

Table 2 Target foil switch TOA data from 13 targets of LS-5.

Target Model No.	Model Description	1st Signal TOA (μs) (Gaseous Jet)	2nd Signal TOA (μs) (Penetrating Jet)	1st and 2nd Signal Time Difference (μs)
1	Std. Straight Pipe	353.9	380.4	26.5
2	Std. Taper Pipe	328.2	364.6	36.4
3	Std. Taper Pipe	323.4	349.5	26.1
4	Std. Taper Pipe/Helix	317.3	341.4	24.1
5	2X Std. Taper Pipe	330.2	357.8	27.6
6	2X Std. Taper Pipe	348.2	366.2	18.0
7	2X Std. Taper Pipe/Helix	342.8	377.8	35.0
8	4X Std. Taper Pipe	350.2	364.6	14.4
9	4X Std. Taper Pipe	340.1	364.9	23.8
10	4X Std. Taper Pipe/Helix	347.7	368.6	20.9
11	Straight Pipe/Expansion Chamber	326.8	381.8	55.0
19	Std. Taper/HURON LANDING Helix	307.6	333.3	25.7
20	Std. Taper/Foam-Lead Helix	328.5	350.4	21.9

Two redundant gages were used on each target to verify that similar pressure signals would be recorded at the same monitoring location, but, as can be seen from the gage signals shown in Figure 15, that was not the case. Ouite different pressure signals were recorded, even from the gages located on the same target. Any future tests with these pressure gages should have the gages remounted to eliminate the possibility of early pressure loss.

3.5 TARGET RATE OF PENETRATION

The target pins yield few data about the penetration rate because of the small amount of target penetration that occurred on the instrumented models. The target used for Model 1 (standard straight pipe) showed no penetration, as will be discussed in the next section. The target for Model 2 (standard taper) showed a total penetration of only 3.5 cm and only three signals were recorded. The final target instrumented with these diagnostics was placed on Model 6 (2X standard taper). These data points are plotted in Figure 13 with the jet ionization pin and target foil switch data. Target penetration occurred at times similar to those measured in the LS-4 experiment. The calculated penetrating jet velocity in the LOS model of 0.57 cm/µs is consistent with the LS-4 data.
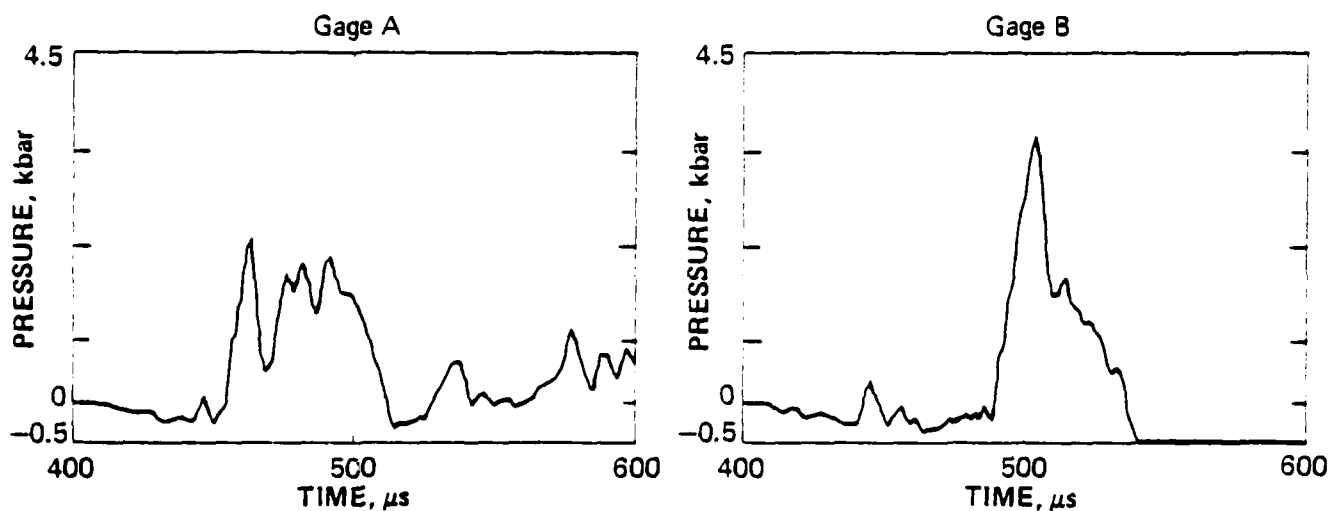
3.6 TARGET DAMAGE

All of the aluminum targets were recovered from this experiment. The crater depths and volumes were measured and photographs taken before and after sectioning the targets. The measured penetration depths and volumes are summarized in Table 3.

STANDARD STRAIGHT PIPE (MODEL 1)

Gage A

Gage B
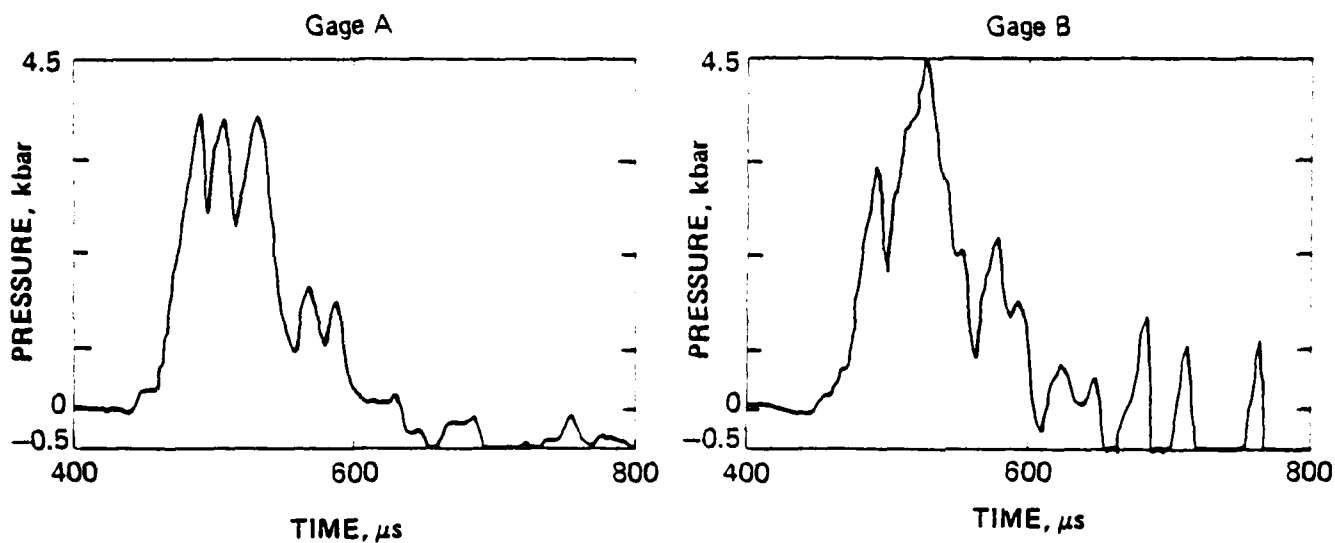
STANDARD TAPER PIPE (MODEL 6)

Gage A

Gage B

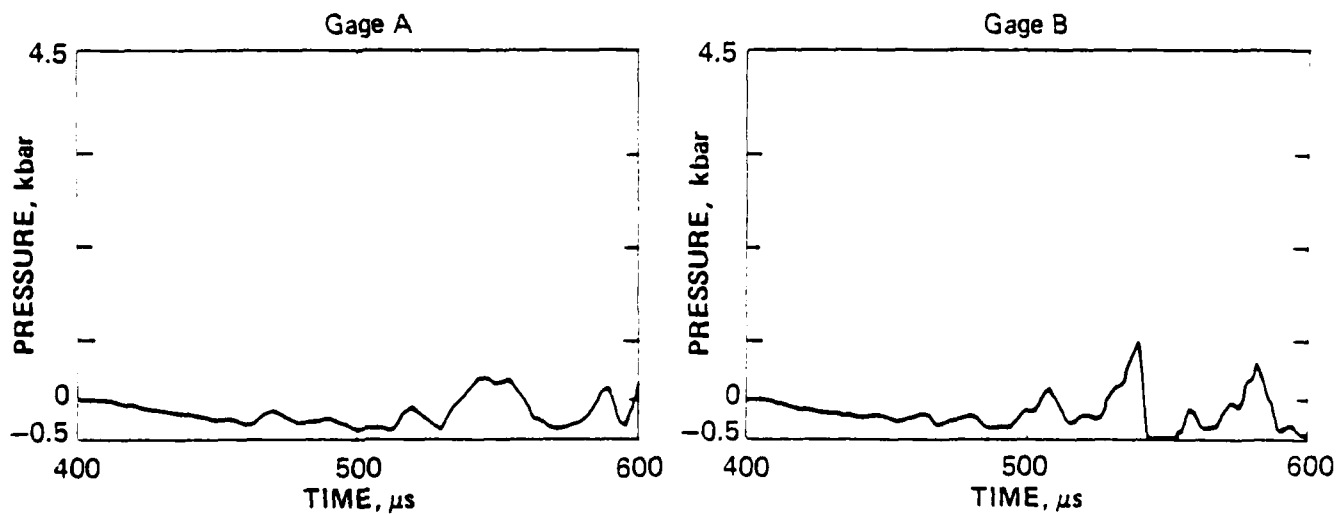## STANDARD TAPER PIPE/HELIX (MODEL 7)

Gage A

Gage B

Figure 15. Comparison of quartz pressure gage signal recorded for Models 1, 6, and 7 on Experiment LS-5.

39

Table 3   Summary of target damage resulting from the various
LOS models used in Experiment LS-5.

LOS Model Type and Description	Model Number	Penetration Depth (cm)	Hole Volume (cm³)	Model Inspection Notes*
Straight Models				
Standard	1	0.0	< 0.1	N.I., poor vacuum
2/3 standard diameter	17	5.1	7.7	1/2 dia. sag
2/3 standard diameter	18	5.1	9.4	1/4 dia. sag
standard/solid rings	12	4.5	7.6	1 dia. dogleg
standard/wire helix	13	10.2	17.4	1/10 dia. sag
standard/soldered helix	14	1.2	0.6	straight
standard/loose rings	15	4.3	5.0	straight
standard/expansion chamber and rings	16	0.7	0.8	1/2 dia. sag
Tapered Models				
Standard taper (0.375 deg)	2	3.5	11.0	N.I.
standard taper (0.375 deg)	3	3.5	17.7	Straight
standard taper/helix	4	1.0	1.5	N.I.
standard taper/HURON LANDING	19	0.9	1.3	Straight
standard taper/ext. lead-foam helix	20	2.2	9.4	1/2 dia. sag, poor vacuum
2x standard taper (0.75 deg)	5	3.7	20.3	N.I.
2x standard taper (0.75 deg)	6	2.8	14.8	N.I.
2x standard taper/helix	7	1.4	3.2	N.I.
2x standard taper/rings	11	1.0	5.3	Straight
4x standard taper (1.5 deg)	8	3.2	18.8	Straight
4x standard taper (1.5 deg)	9	2.4	18.8	N.I.
4x standard taper/helix	10	1.9	19.3	N.I.

*Visual inspection and estimate of straightness. N.I. means "not inspected."

Just prior to firing the test, a number of the targets were removed from the LOS pipes and the condition of the LOS pipes was evaluated. This evaluation was undertaken because of the misfire that occurred on the first attempt to detonate the nitromethane sphere. The conditions observed are noted in Table 3. Of particular importance is the fact that Models 1 and 20 had very poor vacuums, a condition we suspect was caused by water vapor. The target on Model 20 was easily removed and, upon examination, was found to contain water drops. The target was dried out and reattached, but the vacuum remained poor (> 1000 microns). Model 1 was not inspected because of extreme difficulty in removing the bolts from the mounting flange. Both of these models were placed on a separate vacuum pump so as not to compromise the vacuum on the other models. The probable source of water leakage on Model 1 was through the jet velocity pins that penetrated the pipe wall, and the leakage on Model 20 was probably through the welded seam.

The other models that showed the most significant deviations were those that used heavy expansion chambers requiring supports to the bottom of the tank floor. The firing of the MDF on the initial attempt to conduct the test provided sufficient impulse into the models that even the targets were displaced a few centimeters when they were not bolted to the LOS pipe models. This misfire was most unfortunate, and the perturbations to some of the LOS pipes tend to confuse the results.

3.6.1 Standard Model (Model 1). One of the most surprising results of this experiment was that from Model 1. From all indications obtained from jet velocity, target arrival data, and

pressure gage records, the target damage for this model should have shown target penetration similar to that obtained from the eight standard models tested in previous experiments. However, as shown in Figure 16, there was little damage in the central region of the target. The outline of the mounting flange is clearly imprinted on the target face along with other damage occurring during late time launch of the target. The previous average penetration depths and volumes for similar models were 4.85 cm and 17.8 cm^3, respectively. As stated previously, this model had a poor vacuum, which we speculate was caused by water vapor leakage through the jet velocity pins. How much water was present is unknown because the model and target were not disassembled prior to our firing the experiment.

3.6.2 <u>0.375-Degree Half-Angle (STD) Taper Models (Models 2, 3, 4, 19, and 20).</u> Models 2 and 3 had 0.375-degree tapers with no internal helices. They both showed maximum depths of 3.5 cm; the volume was 11.0 cm^3 for Model 2 and 17.7 cm^3 for Model 3. The craters were of a ring-like character with the maximum diameter approximately equal to the diameter of the tube at the target.

Model 4 contained a loose helix with a fixed width and pitch distance similar to that used in the previously tested straight tubes. The crater damage was reduced to 1.0-cm depth and 1.5-cm^3 volume; however, this amount of residual damage was significantly more than measured for straight tubes, where the volume was usually less than 0.3 cm^3. The character of the crater was dramatically changed from circular to axial, possibly suggesting

Figure 16. Photograph of target damage caused by the standard straight model (Model 7) — Experiment LS-5.

that the jet was redirected to the center or that the crater could be caused by the collapse of the helix itself. The targets from Models 2, 3, and 4 are compared in Figure 17.

Model 19 was very similar to the helix proposed for the HURON LANDING event. The Model 19 helix differed from the helix used in Model 4 in that helix width and pitch distance increased in proportion to the tube diameter. The target damage, similar to that for Model 4, had a depth of 0.9 cm and a volume of 1.3 cm^3. These data suggest that either helical design shown in Figure 18 should be equally effective in reducing pipe flow damage but not to the extent anticipated from the straight pipe data.

We tested Model 20 to evaluate whether a thick lead helix wound on the outside of the tapered pipe would reduce target damage by directly altering the collapse process of the pipe. Figure 19 shows that there is less target damage compared to a similar model with no asymmetries. The character of the target crater is no longer ring-like. It is highly likely that this model contained some water, but the effect that the water had on the results cannot be determined. It should be repeated that for Model 1, which we also suspect contained water, target damage was totally eliminated.

3.6.3 0.75-Degree Half-Angle Taper (2X) Models (Models 5, 6, 7, and 11). Models 5 and 6 with 2X taper models contained no asymmetries. Penetration depths of 3.7 and 2.8 cm and volumes of 20.3 and 14.8 cm^3 were similar to those recorded for the standard
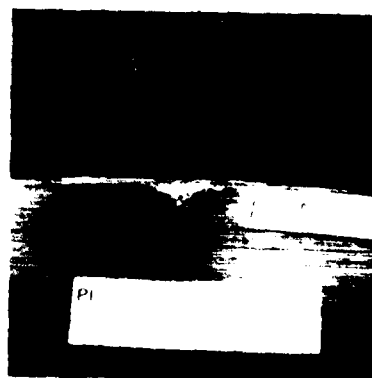
44
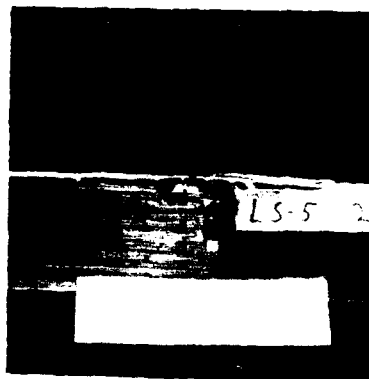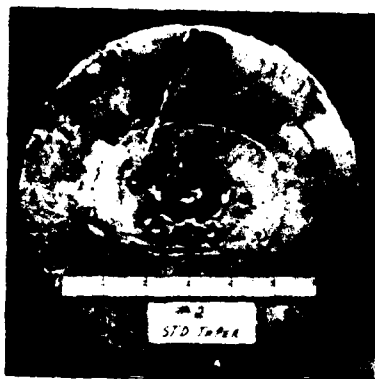
Depth = 3.5 cm
Volume = 11.0 cm³

MODEL 2 (Std. Taper)
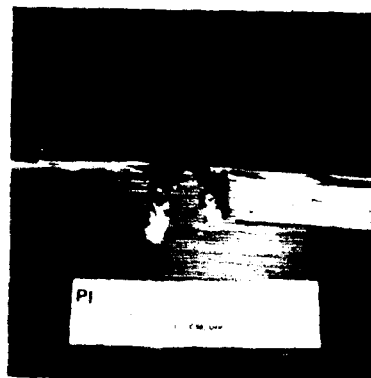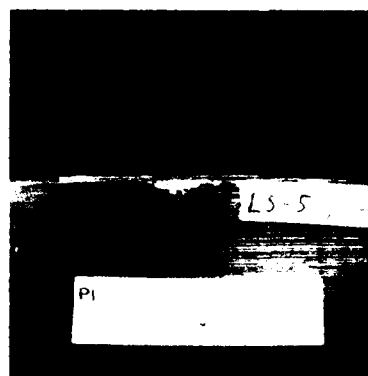
Depth = 3.5 cm
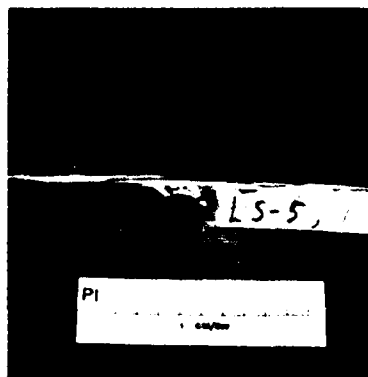Volume = 17.7 cm³

MODEL 3 (Std. Taper)

Depth = 1.0 cm
Volume = 1.5 cm³

MODEL 4 (Std. Taper/Helix)

Figure 17. Comparison of target damage from standard taper models 2, 3, and 4 from the LS-5 Experiment.
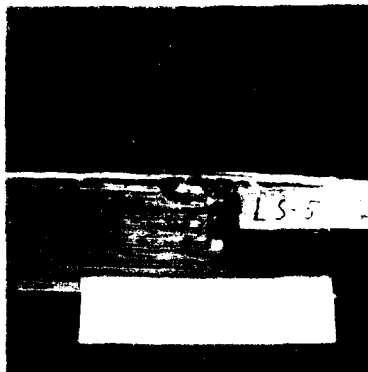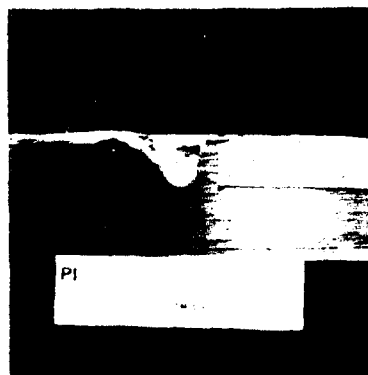
MODEL 4 (Std. Taper/Helix)

MODEL 19 (Std. Taper/HURON LANDING Helix)

Figure 18. Comparison of target damage from Model 4 (std. helix) and Model 19 (HURON LANDING helix).

MODEL 2 (Std. Taper)

Depth   =   3.5 cm
Volume = 11.0 cm^3

MODEL 20 (Std. Taper/External Lead-Foam Helix)

Depth   =   2.2 cm
Volume =   9.4 cm^3

Figure 19. Comparison of target damage from Model 2 (standard taper) and Model 20 (standard taper/external lead-foam helix).

47

taper models. The principal difference was that the ring crater outer diameter increased to a diameter approximately equal to that of the tube diameter at the target.

The use of a helix on Model 7 decreased the total penetration to 1.4 cm with a volume of 3.2 cm^3. Again, damage was primarily confined to the central portion of the target. Target damage for Models 5, 6, and 7 is shown in Figure 20.

Model 11 used rings instead of a helix as the asymmetry. The resultant target damage of 1.0-cm penetration with a volume of 5.3 cm^3 was a little larger than that for the models with a 2X taper helix but not significantly so. These data suggest that helices are slightly better than rings in attenuating the high energy jet. Target damage for this model is compared in Figure 21 with the target from Model 7, which had a helix.

3.6.4 1.5-Degree Half-Angle Taper (4X) Models. Target damage from the 1.5-degree half-angle models is shown in Figure 22. Recorded depths were 3.2 and 2.4 cm for Models 8 and 9, respectively, and the volumes were 18.2 and 18.8 cm^3, not significantly different from damage measured for the models with smaller tapers.

The model with a helix (Model 10) did not show any reduction in target damage. The crater volume was 19.3 cc. Again, as with the standard tapered models, the damage was in the central portion of the target and not shaped like a ring.
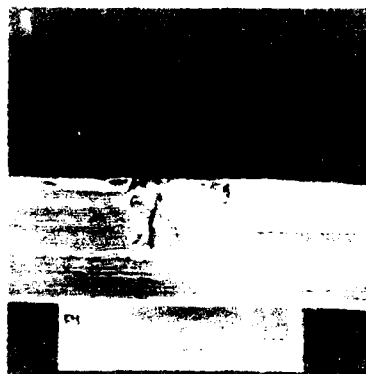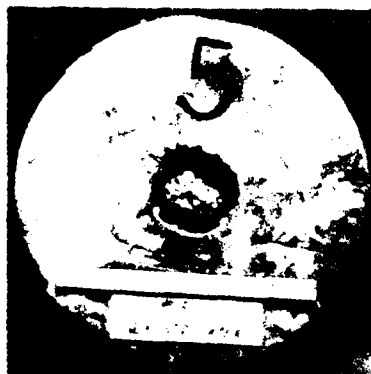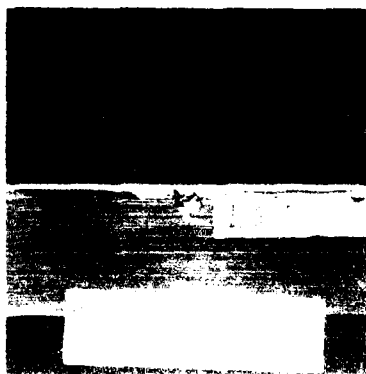
MODEL 5 (2X Taper)

Depth   =   3.7 cm
Volume = 20.3 cm^3

MODEL 6 (2X Taper)
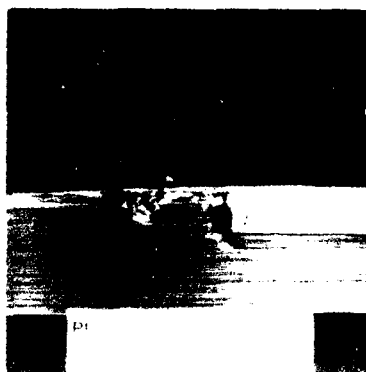
Depth   =   2.8 cm
Volume = 14.8 cm^3

MODEL 7 (2X Taper/Helix)

Depth   =   1.4 cm
Volume = 3.2 cm^3

Figure 20. Comparison of target damage from 2X standard taper models.

49
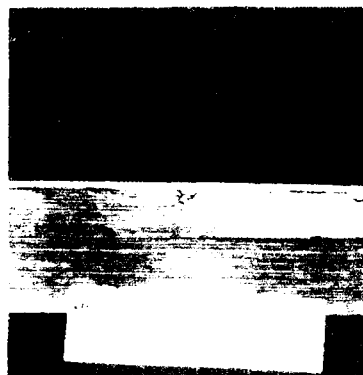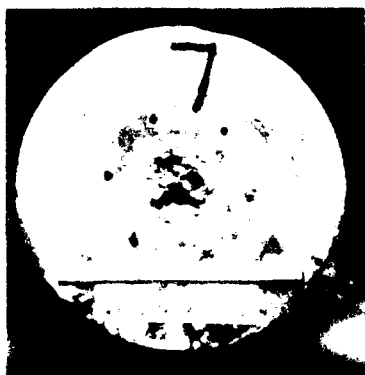
MODEL 7 (2X Taper)

Depth = 1.4 cm
Volume = 3.2 cm³

MODEL 11 (2X Taper/Rings)
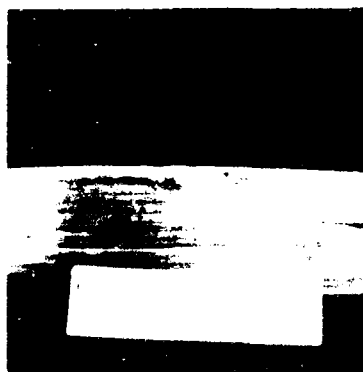
Depth = 1.0 cm
Volume = 5.3 cm³

Figure 21. Comparison of target damage from Model 7 (2X taper) and Model 11 (2X taper/rings).

Depth   =   3.2 cm
Volume = 18.2 cm^3

MODEL 8 (4X Taper)

Depth   =   2.4 cm
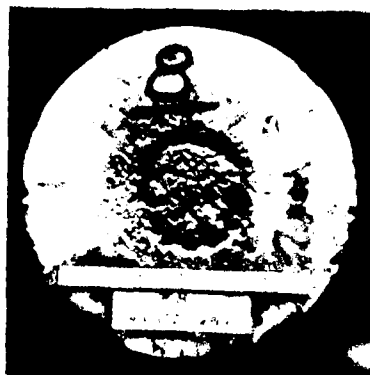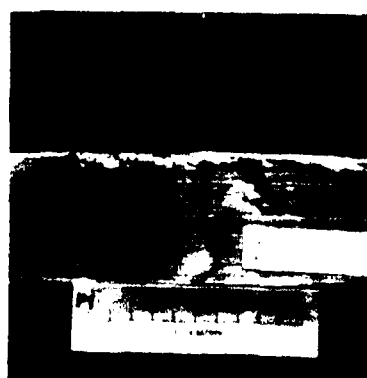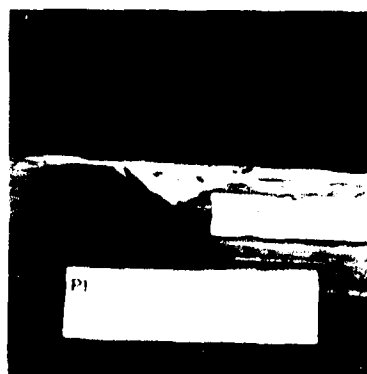Volume = 18.8 cm^3

MODEL 9 (4X Taper)

Depth   =   1.9 cm
Volume = 19.3 cm^3

MODEL 10 (4X Taper/Helix)

Figure 22. Comparison of target damage from 4X taper models from Experiment LS-5.

These data suggest that the helix is becoming less effective as the model taper is increased. The helix changes the damage from a ring-like crater to central damage, which could actually be caused by the collapse of the helix itself.

The photograph shown in Figure 23 compares the target damage for a straight tube (Model 1 of LS-4) with the three different tube tapers.

3.6.5 Straight Tubes with Asymmetries. The results of the tests of the straight tubes with asymmetries were somewhat surprising, and any conclusions must be conditioned somewhat because of model misalignment and damage that occurred when the experiment misfired. The results of these tests are to be compared with previous tests with helices, which produced crater volumes of less than 0.3 cm^3.

Model 13, with an internal helical soldered wire as the asymmetry showed no reduction in jet penetration (see Figure 24). These data suggest that a thin width asymmetry inside the tube is insufficient to attenuate the jet.

The helix for Model 14 was soldered to the wall to determine the effect of firmly attaching the helix. In previous experiments the helices were loosely placed in the tubes. The resultant crater depth of 1.2 cm and volume of 0.6 cm^3 shown in Figure 24 would indicate that some motion of the helix prior to jet arrival is required to cause total jet attenuation. This penetration crater volume was much smaller than the average of the

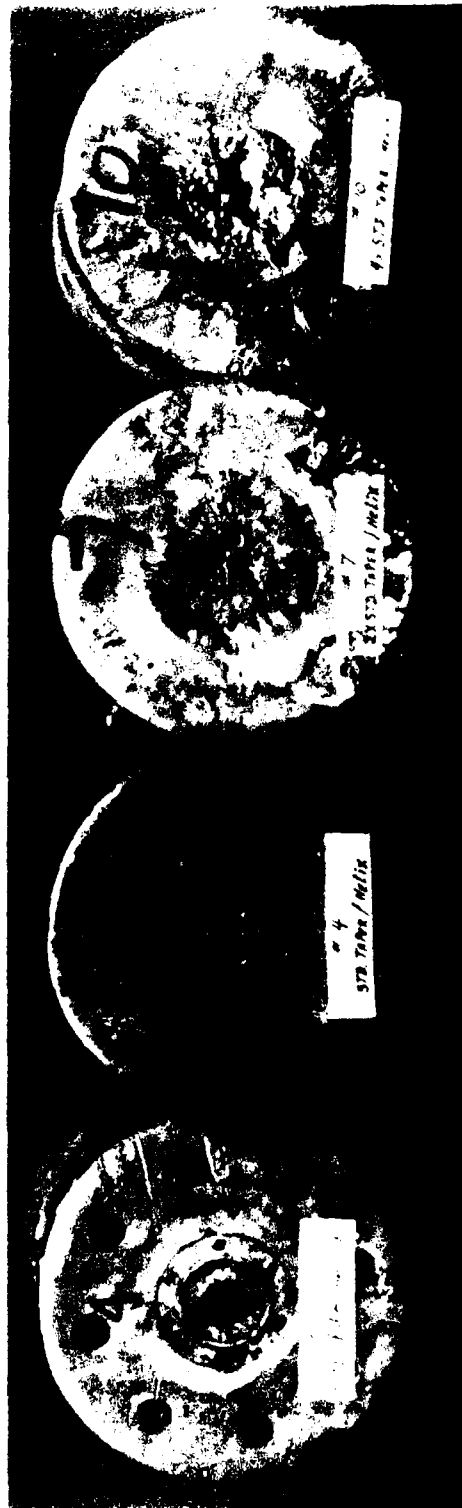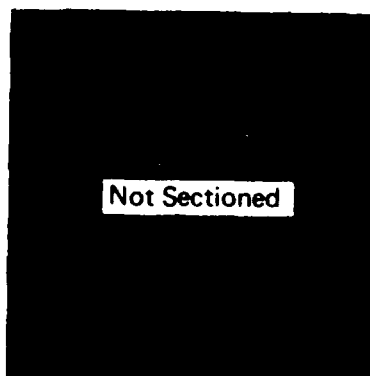Figure 23. Comparison of straight and tapered LOS pipes with and without the standard internal helix.

Depth = 10.2 cm
Volume = 17.4 cm³

MODEL 13 (Soldered Wire Helix)

Not Sectioned

Depth = 1.2 cm
Volume = 0.6 cm³

MODEL 14 (Soldered Helix)

Figure 24. Comparison of target damage from standard straight models with a wire helix (Model 13) and a standard helix soldered to the tube (Model 14).

volumes from the standard LOS pipe models, however, indicating that tipping of the helix into the flow is not the sole attenuation mechanism.

Model 15 had loose rings as the asymmetry to compare the results with loose helices. The target crater depth of 4.3 cm and volume of 5.0 cm^3 suggest that rings are not as effective as helices, similar to the results with tapered pipe models. Model 12 was fabricated with solid rings to further evaluate whether motion of the asymmetry prior to the high energy jet arrival was important in jet attenuation. The resultant crater depth of 4.3 cm and volume of 5.0 cm^3 were similar to those observed for Model 15 (loose rings), providing further evidence that motion of the asymmetry is required for effective jet attenuation. A significant dogleg ($\sim$ 1.9 cm) in this model occurred where the straight section of the pipe was attached to the ring asymmetry section. No estimate of the effect of the dogleg on the results can be readily made. The crater damage for these two targets is shown in Figure 25.

Model 16 used an expansion chamber with rings protruding slightly below the inside surface of the straight tube section. In the LS-4 experiment, a similar model was tested except that the inner diameter of the rings was the same as the inner diameter of the tube. In that test, little attenuation of the jet occurred. The target for this model, however, showed rather good reduction in the crater damage. The recorded crater depth was 0.7 cm with a volume of 0.8 cm^3. The result of this test is not
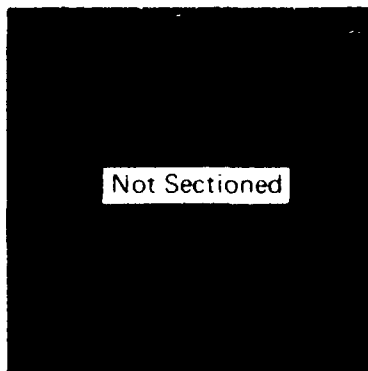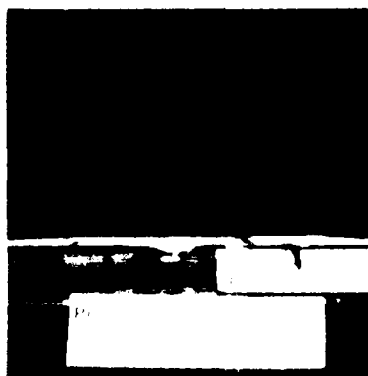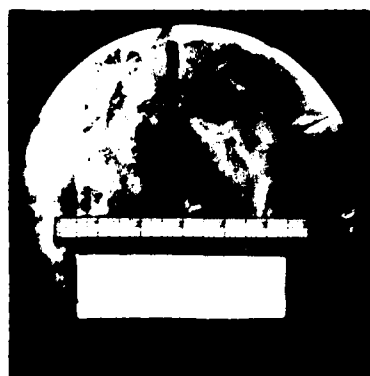
Depth   = 4.3 cm
Volume = 5.0 cm³

MODEL 15 (Loose Rings)
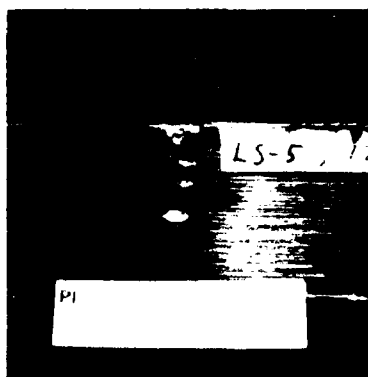
Depth   = 4.5 cm
Volume = 7.6 cm³

MODEL 12 (Solid Rings)

Depth   = 0.7 cm
Volume = 0.8 cm³

MODEL 16 (Expansion Chamber with Rings)

Figure 25. Target damage from Models 15, 12, and 16 for the LS-5 Experiment.

consistent with the results observed for Models 12 and 15, where much larger craters were measured, and cannot be readily explained. The target from this model is shown in Figure 25.

3.3.6 <u>Two-Thirds Diameter Models (Models 17 and 18)</u>. Models 17 and 18 used tubes whose diameters were two-thirds of the diameters of standard pipes previously tested. Model 17 produced a crater 10.1 cm deep with a volume of 7.7 cm^3. The depth of Model 18 was 5.1 cm with a volume of 9.4 cm^3. The depths were above the average recorded for standard diameter pipes while the volumes were below the average, slightly beyond one standard deviation. As can be seen from the target photographs shown in Figure 26, the crater shapes are quite different.
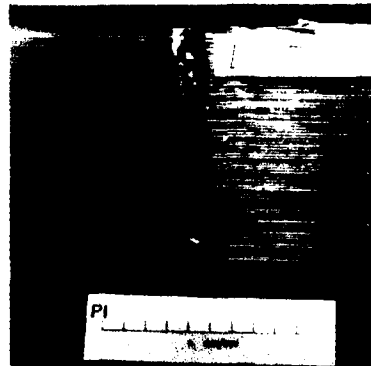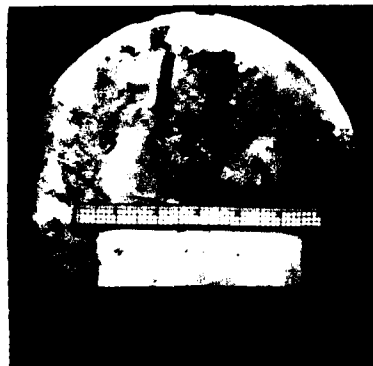
Depth = 10.1 cm
Volume = 7.7 cm³

MODEL 17 (2/3 Std. Tube dia.)
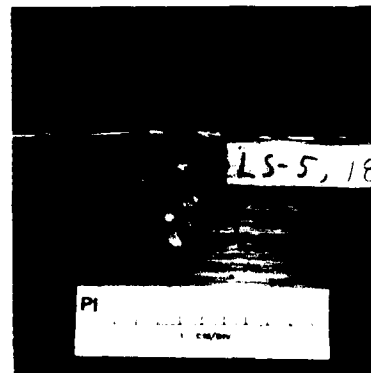
Depth = 5.1 cm
Volume = 9.4 cm³

MODEL 18 (2/3 Std. Tube dia.)

Figure 26. Target damage from 2/3 scale standard straight pipes (Models 17 and 18) of Experiment LS-5.

58

SECTION 4

SUMMARY OF RESULTS

The major findings of the LS-5 experiment were:

- The penetration craters formed by the tapered LOS pipe
  models were similar in volume to the standard straight LOS
  pipe craters, but all had a distinct ring-like character
  with the ring diameter corresponding to the pipe diameter
  at the target. This finding suggests that the penetrating
  jet flows along the wall of the LOS pipe.

- Internal helices are slightly less effective in eliminat-
  ing target damage in LOS pipes with a 0.375-degree half-
  angle taper than in straight LOS pipes. They become less
  effective in attenuating the jet as the taper angle
  increases, becoming totally ineffective at a 1.5-degree
  half-angle. The craters are no longer ring-like, however,
  with damage located in the center of the target.

- The HURON LANDING helix (variable width and pitch dis-
  tance) was as effective as the standard helix (constant
  width and pitch distance) in eliminating target damage.

- A standard, straight tube LOS model (Model 1) without any
  internal asymmetry to attenuate the penetrating jet pro-
  duced no crater (Model 1). This surprise result is
  contrary to results obtained on four previous experi-
  ments. It was known prior to the test that this model
  could not be evacuated to the normal 0.1-micron vacuum and
  probably contained some amount of water vapor or liquid.
  It is not known at this time if water in the pipe will
  indeed act as such an effective attenuator.

- Helical and ring asymmetries are less effective when firmly attached to the wall of straight tube LOS models.

- Helices appear to be more effective than rings in attenuating high energy jets.

In addition to the findings given above, additional results were obtained from the active instrumentation placed on selected models and targets. The test bed TOA data showed that the test bed was well saturated. Gaseous jet velocities were obtained that were consistent with valid data from previous experiments. Jet pressure signatures obtained were not interpretable. Flat foil switches placed on the target appear to provide good TOA data for the gaseous jet but do not report interpretable TOA data for the penetrating jet consistent with target penetration data.

Most surprising was the fact that all electronic measurements recorded for Model 1 (standard straight tube without any asymmetry) indicated that a normal crater should have formed. No crater was observed on the recovered target.

REFERENCES

1. E. T. Moore, Jr., and R. Funston, "Asymmetric Collapse of LOS Pipe," DNA Report DNA 5023F (July 1979).

2. E. T. Moore, Jr., and R. Funston, "Asymmetric Collapse of LOS Pipe," DNA Report DNA 5322F (May 1980).

3. D. Mumma, J. Thomsen, R. Funston, and E. T. Moore, Jr., "Asymmetric Collapse of LOS Pipe," PIFR-1403, Physics International Company (March 1982).

DEPARTMENT OF DEFENSE

Defense Nuclear Agency
     ATTN: SPTD, T. Kennedy
4 cy ATTN: TITL

Defense Technical Information Center
12 cy ATTN: DD

Field Command
Defense Nuclear Agency
     ATTN: FCTT, G. Ganong
     ATTN: FCTT, W. Summa
     ATTN: FCT, Col G. Ballantine
3 cy ATTN: FCTK, B. Ristvet
3 cy ATTN: FCTK, C. Keller

DEPARTMENT OF ENERGY

Nevada Operations Office
     ATTN: R. Newman

OTHER GOVERNMENT AGENCY

Department of the Interior
US Geological Survey
     ATTN: R. Carroll
     ATTN: A. Fernald

DEPARTMENT OF ENERGY CONTRACTORS

Desert Research Institute
     ATTN: D. Schulke Sec Off for P. Fenske
     ATTN: D. Schulke Sec Off for C. Case

University of California
Lawrence Livermore National Lab
     ATTN: B. Hudson
     ATTN: F. Morrison
     ATTN: L-209, G. Higgins
     ATTN: R. Terhune
     ATTN: L. Makague

DEPARTMENT OF ENERGY CONTRACTORS (Continued)

Los Alamos National Laboratory
     ATTN: T. Kunkle, ESS-5
     ATTN: R. Brownlee
     ATTN: C. Keller
     ATTN: F. App
     ATTN: B. Travis

Sandia National Lab
     ATTN: C. Smith
     ATTN: Org 7112, C. Mehl

DEPARTMENT OF DEFENSE CONTRACTORS

California Research & Technology, Inc
     ATTN: M. Rosenblatt

Kaman Tempo
     ATTN: DASIAC

Pacific-Sierra Research Corp
     ATTN: H. Brode, Chairman SAGE

Pacifica Technology
     ATTN: D. Patch

Physics International Co
4 cy ATTN: E. Moore
4 cy ATTN: D. Mumma
4 cy ATTN: R. Funston
4 cy ATTN: J. Thomsen

R&D Associates
     ATTN: P. Haas

S-CUBED
     ATTN: R. Duff
     ATTN: C. Dismukes

SRI International
     ATTN: A. Florence